2020

In-vitro Localisation and Degradation of Few-layer MoS2 Submicrometric Plates in Human Macrophage-like Cells: a Label Free Raman Micro-spectroscopic Study

Caroline Moore
Technological University Dublin

Andrew Hrvey
Trinity College Dublin, Ireland

Jonathan N. Coleman
Trinity College Dublin

Hugh J. Byrne
Technological University Dublin, hugh.byrne@tudublin.ie

Jennifer McIntyre
ity College Dublin, Ireland

Follow this and additional works at: https://arrow.tudublin.ie/nanolart

Part of the Pharmacology, Toxicology and Environmental Health Commons

In-vitro localisation and degradation of few-layer MoS$_2$ submicrometric plates in human macrophage-like cells: a label free Raman micro-spectroscopic study

Caroline Moore[1]*, Andrew Harvey[2], Jonathan N. Coleman[2], Hugh J. Byrne[1], Jennifer McIntyre[3]

1. *FOCAS Research Institute, Technological University Dublin, City Centre Campus, Ireland*

2. *Centre for Research on Adaptive Nanostructures & Nanodevices (CRANN) and Advanced Materials and BioEngineering Research (AMBER) Centre, Trinity College Dublin, Ireland*

3. *Department of Education, Trinity College Dublin, Ireland*

* Corresponding author email: C10322785@mytudublin.ie

Abstract

Monitoring the uptake, micro-environment and fate of micro or nano scaled particulate materials in cells is of paramount importance for the emerging fields of toxicology and medicine. Such particulate materials are known to interfere with colorimetric assays and many such assays record only a single end-point. Therefore, there is a need for a label-free, cost effective technique with little or no inference from the particulate materials.

Raman micro-spectroscopy was used to simultaneously interrogate the integrity of few-layer MoS_2 submicrometric plates in human macrophage-like cells, in-vitro, as well as the biochemical characteristics of the local micro-environment in which they are encompassed. Firstly, the degradation profile of MoS_2 plates induced by hydrogen peroxidase was established using UV-Vis absorption and Raman micro-spectroscopy. Raman micro-spectroscopic maps interrogated all aspects of the cell, including the nucleus, cytoplasm and perinuclear region, and the location/distribution of MoS_2 was monitored as a function of time (4, 24 and 72 h). Whereas only pristine MoS_2 was detectable after 4 and 72 periods, degradation in-vitro was confirmed following a 24 h incubation. Analysis of the MoS_2 micro-environments revealed the presence of both phosphatidyl lipidic vesicles and enzymatic regions containing lysozyme, the former being most associated with the MoS_2 degradation. There was an increase and saturation of cytosolic neutral lipids detected following a 24 h incubation with MoS_2, which reduces following a prolonged incubation of 72 h. This study reveals that macrophage-like cells perform degradation of the material in-vitro within lipidic vesicles subsequent to phagocytosis, which manifest as an increase in the production of lipid bodies as a mechanism of defense following exposure to industrial grade MoS_2.

Introduction

The field of 2D materials technology has been growing since the isolation and characterisation of graphene monolayers in 2004(1). Due to the prospect of increased manufacture of 2D engineered materials for flexible transparent displays(2), enhanced energy storage and/or medical applications(3), consideration of the risk and/or potential for human exposure is paramount(4). There is a need to understand how such materials interact with biological cells following exposure, and how, in turn, the cellular micro-environment effects these particles. MoS_2 is one such 2D material which has attracted recent attention due to its enhanced properties over its analogue graphene, based on its electronic band structure (5). Compared to its bulk form (in-direct band gap), MoS_2 has superior properties in its mono or few-layer format, with a direct bandgap, allowing improved catalytic performance in comparison to graphene, which possesses a zero band gap (2,5). Mono or few-layer MoS_2 micro/nano plates can be prepared by liquid exfoliation along with a series of liquid centrifugation steps for size selection(6,7), and is a widely studied material, with increasing interest due to its use as a catalyst in gas evolution, photodiodes and in supercapacitor electrodes. Thus, it is necessary to study how the material interacts with cells, as opposed to bulk MoS_2 which has fewer applications.

When a pathogen enters the human body, it activates both the innate and adaptive immune response systems to eliminate the threat and reduce the possibility of infection. The first line of defence when exposed to a pathogen is the recognition of pathogen associated molecular patterns (PAMPs) found on bacterial cell walls(8) by pattern recognition receptors (PRRs) which in turn causes the secretion of effector molecules such as cytokines or chemokines from activated immune cells(8). Cytokines have the ability to recruit immune cells to the site of infection, stimulate neighbouring cells to produce additional cytokines or encourage cell maturation/growth(9).

Macrophages play a crucial role in recognising PRRs to cause a cascade of events designed to eliminate a foreign threat from their environment and to maintain homeostasis(8). Macrophages are proficient in recognising PRRs, engulfing the pathogen in a process termed phagocytosis, degrading the foreign threat while also having the capability to produce

cytokines to further enhance the immune response(8). Following the identification of a foreign substance, macrophages reduce motility and increase their ability to carry out phagocytosis(10). Actin rearrangement allows for the pathogen/material to be surrounded by pseudopodial extensions and internalised in a double membrane early phagosome (pH 6.2)(11). Later, this phagosome will bind with an acidic lysosome (pH 4.5) to form a single membrane phagolysosome (pH 5.2)(11). Alternatively, foreign bodies can be internalised in macrophages by non-phagocytic pathways, including clathrin-mediated endocytosis, caveolin-mediated endocytosis or micropinocytosis. Although the early uptake mechanism can differ slightly for each pathway, Xianbing Zhu *et al.* have shown that vesicles from the non-phagocytic uptake pathway are ultimately destined to accumulate within lysosomes (12). In order to achieve homeostasis, macrophages play a role in innate immunity and the activation of other immune cells by the process of the micro or nano particulate uptake, degradation, antigen presentation and cytokine production(13).

A variety of micro/nano particles are known to evoke an immune response, once in contact with cells, and this is due to the particle being recognised as a foreign substance due to unfamiliar molecular patterns. Studies of the uptake and location of pristine graphene in macrophage-like cells have shown that the material is contained within lysosomal compartments(14), a cellular mechanism for digestion of foreign bodies. Peroxidase enzymes such as myeloperoxidase (MPO) are found in-vitro within azurophilic granules and are known to contribute to the degradation of material(15–17). Although no degradation of pristine graphene was reported(14), the degradation of single walled carbon nanotubes (SWCNTs) has previously been studied in-vitro using changes in the D and G Raman bands as indications of degradation(18). Kurapati *et al.* have shown no major differences between the degradation from biologically relevant enzymes or chemical degradation of MoS_2 up to 30 days although the hydrogen peroxide ex-vivo degradation occurred at a faster rate(19). A review written by Bhattacharya *et al.* has highlighted the corona formation on the surface of carbon based nanoparticles can affect the bio-distribution, catabolisation and ultimately the process in which cells and immune systems interact with the particulate material (20). It has also been shown that coating the particle surface with biocompatible substances such as poly-ethyl glycol (PEG) can aid in "camouflaging" it from immune cells(21). This method can reduce the removal or degradation of the material and improve circulation time throughout the body.

When MoS_2 micro/nano particles are in close proximity to macrophages, the surface of the unmodified material will be recognised as a foreign threat and an immune response will be initiated to remove it from circulation. This study investigates the effect of a sub-lethal dose of MoS_2 on macrophage-like cells and monitors the stability and degradation of the material in-vitro, primarily using confocal Raman micro-spectroscopy. Raman spectroscopy functions by using a monochromatic light source that interacts with molecular vibrations within the sample to cause a Raman shift which provides detailed information about the vibrational modes within the given sample[22]. Spectral mapping using confocal Raman micro-spectroscopy allows high resolution, in-depth information to be retrieved from an identified area within the cell to examine the material integrity, cellular compartmentalisation, particulate uptake and/or subcellular location[23]. While point spectra acquired by Raman spectroscopy have historically been used for detailed analysis of the specific biochemical responses of cells[24], the technique used here presents the additional benefit of simultaneously monitoring the integrity of the MoS_2 material [25]. Spectra are collected at each step with the use of an automated stage to generate images of pseudo colour coded clusters based on spectral similarities or differences. The biochemical composition of various organelles can be determined by Raman spectroscopy without the addition of fluorescent labels, making it a cost effective, non-destructive and label-free method[26] to monitor the exposure of cells to particulate materials [23,27].

Raman has been successfully used to study the structure of nanomaterials[28], shifts due to applied stress[29] or examining layers with 2D materials[25,30]. First order Raman bands associated with the E^1_{2g} (in-plane) and A_{1g} (out-of-plane) vibrational modes within the MoS_2 layer are observed at approximately 380 and $407 cm^{-1}$ respectively[25]. An excitation source of wavelength 532 nm means that these modes are resonantly enhanced[31], and therefore prominent against the background Raman fingerprint of the cell in the region of 500-$1800 cm^{-1}$, such that the cellular micro-environment and the material integrity can be monitored simultaneously. Second order Raman bands for MoS_2 are also detectable in the region ~500 - $800 cm^{-1}$,[31] and, although they are weak compared to the first order bands, they can interfere with interpretation of the biological spectral signature of the cell, limiting the useful analysis range for the latter to $800-1800 cm^{-1}$.

Our collaborating group from Trinity College Dublin, led by Professor Jonathan Coleman (co-author), has published extensively on the production and synthesis of an array of 2D materials. Their protocols reliably yield reproducible, stable and well characterised exfoliated materials. A lot of work in the past has also been published by our collaborating group on characterising the size distribution of MoS_2 dispersions prepared by Liquid Cascade Centrifugation (LCC) (32). Due to this, it is very simple to determine the particulate lateral size (length) along with the number of monolayers per particle (thickness) using UV-vis spectroscopy (33). Due to the nature of liquid phase exfoliation, a relatively polydisperse sample is produced with a broad distribution of both lateral dimensions and thickness which need to be further processed for size selection. Additionally, the known size selection techniques produce a low yield of the size selected particulate material. Therefore, LCC was developed to produce high yields of 2D materials at a predetermined lateral size at high concentrations. Furthermore, this technique is applicable for a vast array of 2D materials prepared in surfactants.

Previously, the cytotoxicity, uptake and inflammatory responses of few layered MoS_2 nanometric and submicrometric plates were investigated (34). (Note, the nomenclature used is chosen in accordance with an updated naming system for 2D materials (35,36)). Three lateral sizes of micro/nanoplates (50, 117 and 177 nm) were exposed to three cell types, mimicking three possible exposure routes (A549:inhalation, AGS:ingestion and THP-1:blood circulation)(34). A range of concentrations were tested, establishing sub-lethal dose regimes of 1 μg/ml, THP-1 cells being seen to be susceptible to toxicity due to its cellular function as a phagocytic cell. Confirmation of uptake was observed of all material sizes in all three cell types using Transmission Electron Microscopy (TEM). Therefore, in order to further investigate the uptake and sub-cellular location of a sub-lethal dose of particulate MoS_2 in THP-1 cells, Raman micro-spectroscopy has been employed. For the purpose of tracking the movement and/or location of MoS_2 following internalisation, a pulse chase exposure method was applied(37), whereby cells were initially exposed to MoS_2 containing culture medium for 4h to allow sufficient time for internalisation, and subsequently incubated in media containing no MoS_2 for 4, 24 or 72 h.

Materials and methods

2D MoS$_2$ Production

Full characterisation of MoS$_2$ material fabricated by the same method has been published previously (7,38,39). The stability of few-layer MoS$_2$ submicrometric plates in surfactant over time has been reported as -40 mV(7). MoS$_2$ production is briefly outlined below.

MoS$_2$ powder (Sigma Aldrich, Ireland) was sonicated in aqueous surfactant solution (sodium cholate (SC), 6 g/l) for 1 h. To remove any impurities in the starting powder, the resultant dispersion was centrifuged at 5 krpm for 90 min. Having discarded the supernatant, the sediment was re-dispersed in fresh aqueous SC solution (0.5 g/l) and was sonicated for 6 h to produce a stock dispersion. This stock dispersion was relatively polydisperse, and to achieve a better-defined particulate size distribution, the sample was subjected to liquid cascade centrifugation (LCC).

LCC involves a series of progressively increasing centrifugation speeds to produce a narrow distribution of plate sizes in suspension(32). The stock dispersion was initially centrifuged at 1 krpm for 90 min to remove any unexfoliated material. The sediment was discarded, while the supernatant was collected and centrifuged at a higher speed (1.5 krpm for 90 min). After centrifugation at 1.5 krpm, the sediment was collected and redispersed in fresh aqueous SC (0.5 g/l), which represents the first particulate size selection. The supernatant was then subjected to further centrifugation at the next highest speed, 2.5 krpm, for 90 min. Similarly, the sediment was collected and redispersed in aqueous SC, while the supernatant was centrifuged at a higher speed. This process was repeated for 2.5 krpm, 3.5 krpm, 5 krpm and 10 krpm. The respective sediments for a given speed were analysed using UV- vis spectroscopy and electron microscopy to determine the particulate concentration, mean lateral size and layer number (40). LCC maximises the micro/nano plate concentration of sheets in suspension (32).

The size and thickness were estimated according to the protocols previously described (33). For the batch employed in the current studies, the lateral size and numbers of layers was

estimated using UV-visible absorption spectroscopy (UV-Vis) to be 120±20 nm and 3-5 layers, respectively.

Cell Culture

Human acute monocytic leukemia (THP-1) cells were cultured in Roswell Park Memorial Institute (RPMI) medium (Gibco, Bio-sciences Ltd, Ireland). RPMI was supplemented with 10% Foetal Bovine Serum (FBS). Cells were maintained in a humidified atmosphere at 37 °C and 5% CO_2. THP-1 monocytic cells were seeded onto calcium fluoride (CaF_2) discs (Crystran, United Kingdom) at a concentration of 1 x 10^5 cell/ml (3 ml/sample) and differentiated into macrophage-like cells by incubating them with 100 nM phorbol 12-myristate 13-acetate (PMA) for 72 h.

Cellular Preparation for Raman Mapping

To ensure the acquisition of high-quality spectra, sample preparation and measurement conditions were optimised. Subsequent to optimisation of the Raman protocol, THP-1 cells grown on CaF_2 discs were exposed to a sub-lethal dose of 1 µg/ml of MoS_2 (105 nm) for 4 h to allow sufficient time for internalisation and then cells were incubated in supplemented media (no particulate material present) for a specified amount of time (4, 24 and 72 h). Free SC surfactant solution was not tested as a control, as the molecular organisation and concentration in solution is non-comparable to the SC bound to plate edges to aid in stabilization. The equivalent concentration of SC found in micro/nano material suspensions was previously tested showing minor effect on three cells types (34). The reagents used were not endotoxin free, although the cellular response to endotoxin was seen to be plate dependent, as described in our previous publication (34). It was observed that cytokine production in both the three cell lines tested (A549, AGS and THP-1) along with bone marrow derived dendritic cells (BMDC's) were plate size dependant, the smallest particles of lateral dimensions ~50 nm eliciting the highest response. It should be noted that a relationship between the quantity of endotoxin detected and the available surface edge was observed. MoS_2 has discrete Raman bands at ~ 381 and 407 cm^{-1} (31) which do not overlap with any cellular information, therefore the presence of these bands confirms uptake and facilitates the exploration of its intracellular integrity. Following incubation, cells were washed twice with pre-warmed phosphate buffer

saline (PBS) and fixed in 4% Formalin (3 ml/sample) for 15-20 min at room temperature. Subsequent to fixation, cells were washed twice with Millipore water and left in water for Raman micro-spectroscopy.

Raman Spectroscopy of THP-1 cells

Raman spectra were recorded using a Horiba Jobin-Yvon LabRAM HR800 spectrometer equipped with a 532 nm solid state diode laser (50 mW), narrow bandwidth version with single edge filter and 600 gr/mm line grating. The Horiba Jobin-Yvon LabRAM HR800 spectrometer is a dual Raman microscope with the capabilities to measure samples in both upright and inverted mode, the upright microscope using the standard Olympus BX41 model, while the inverted model is Olympus IX71. Raman measurements for both MoS_2 degradation and biological samples were analysed using the same Raman instrument. All cellular measurements were acquired in water with a 100x water immersion objective (LUMPlanF1, Olympus) with a spot size of 1 μm, using the upright BX41 model. Raman maps were recorded over a spectral range from 300 to 1800 cm^{-1}. Spectra were recorded 15 sec acquisitions and 2 accumulations. Cells were grown on a calcium fluoride (CaF_2) substrate, which has minimal background contribution with only a distinct band present at 321cm^{-1} which does not overlap with particulate material or cellular information (41).

Subsequent to Raman acquisition, data was analysed using a Factor Analysis (FA) algorithm (Labspec 5) and classical least squares (CLS) analysis with Labspec software version 6(42). To ensure spectra are of good quality, data was smoothed with a Savitzky-Golay filter, spectra were cut to the desired spectral range (365-1800cm^{-1}, 800-1800cm^{-1} and 365-470cm^{-1}) and baseline corrected. The factor analysis (FA) algorithm is used to classify spectra within a Raman map dataset based on different spectral features into different clusters/factors. FA is an unsupervised method of processing spectral images to identify similar spectral profiles within a Raman map dataset (e.g. MoS_2 peaks, cellular features). FA works by randomly assigning centroids to a once anonymous data set to achieve clusters in which no overlap of centroids is occurring. Each spectral point is classified based on the nearest centroid centre. The mean spectra for each cluster are displayed as Factors in Figure 2 – 6. CLS analysis then fits weighted contributions of each of the chosen factors (mentioned above) to each point in the map. The location/distribution of each cluster is produced and given a pseudo-colour for effective visualisation and therefore the distribution and location and/or integrity of MoS_2 within the

cells can be determined. Subsequent to unsupervised FA (Labspec 5) and supervised CLS (Labspec 6), the data is then subjected to further pre-processing in Matlab. A water contribution was weighted and subtracted from each cluster prior to principal component analysis (PCA), in order to monitor the evolution of the surrounding micro-environment of MoS_2 over time. For further identification of components, an in-house dataset of 82 standards was compared to PCA loadings. A weighted spectrum is calculated by subtracting one standard from another (e.g. Phosphatidyl lipid minus Lysozyme) and then direct comparison with PCA loadings.

MoS_2 degradation with H_2O_2

The sample of few-layer MoS_2 submicrometric plates was diluted to a final concentration of 100 μg/ml in 5 mls of PBS. Hydrogen peroxide was then added to each vial to have a final concentration of 0, 10, 500, 1000 and 2000 μM. Samples were then incubated at 37°C, 5 % CO_2 for a total of 14 days. Images were taken at intervals (Day 0, 1, 2, 4, 7 and 14) following a gentle inversion, aliquots were taken and stored in the dark at -80°C until ready for Raman and UV-Vis analysis. Raman samples were placed in Labtek chamber slides and recorded with 60x liquid immersion on an inverted microscope. Spectra were recorded using the Horiba Jobin-Yvon LabRAM HR800 spectrometer in the inverted mode, using an Olympus IX71 microscope. A laser excitation of 532 nm was used examining the spectral range in 300 to 500 cm^{-1}, laser filter 50 %, 3 second acquisition and 10 accumulations. Samples to be analysed using UV-Vis were placed in 96 well plates and absorbance recorded using a SpectraMax plate reader (Molecular Devices, USA). To accurately determine position, area and shape of Raman and UV-Vis peaks, curve fitting was performed in Labspec 5 using Gaussian-Lorentzian curve fitting approach.

Oil Red O Staining

Following incubation with MoS_2 for a specific amount of time (4, 24 and 72 h), the cells were washed and fixed as described in Cellular Preparation for Raman Mapping above, and the samples were allowed to air-dry overnight prior to staining. Oil red O staining was prepared fresh and filtered before staining the cells for 15 min at room temperature (3 ml/ sample). Oil red O was removed, and samples were washed multiple times with distilled water.

Samples were allowed to dry and the coverslips were attached using mounting media. Images were then taken on an Olympus Microscope (BX51).

Results

Induced plate degradation ex-vivo with hydrogen peroxide

Macrophages are known to uptake foreign substances into phagosome/lysosomal compartments, in which material is destined for degradation prior to catabolism/excretion. In order to understand the potential impact of the digestion process on submicrometric plate spectra, MoS_2 (100 µg/ml) suspended in surfactant were chemically degraded over 14 days using H_2O_2 (2000 µM) and monitored by UV-Vis absorption and Raman spectroscopy. Raman spectra of sample aliquots are presented in Figure 1A(i) (Day 0 – blue, Day 1 – green, Day 2 – purple, Day 4 – yellow, Day 7 – cyan and Day 14 – red). Bar charts shown in Figure 1A (ii-v) were derived using the Gaussian-Lorentzian curve fitting algorithm in the Horiba Labspec 5 software. The position of the E^1_{2g} MoS_2 Raman peak at 380 cm^{-1} shows a gradual shift and decrease in intensity (Figure 1A(ii-iii), while the A_{1g} Raman peak at 407 cm^{-1} shows no significant shift (Figure 1A(iv-v)). Notably, a broadening and increase in area can be clearly seen for the 407 cm^{-1} Raman peak. A similar decrease in intensity was observed by Kurapati *et al.*, although over a longer time frame of 30 days[19]. The samples were also analysed using UV-Vis absorption spectroscopy and the corresponding spectra can be seen in Figure 1B(i). An evident decrease in amplitude can be seen for both the lower (~618 nm) and higher (~675 nm) wavelength peaks (Figure 1B (ii and iv)). Noticeably, a decrease in peak area could also be observed over time following plate degradation. No MoS_2 material can be detected by UV-Vis following a 14-day incubation in H_2O_2 and consequently the curve fitting could not be applied. This would suggest that all material has been degraded by H_2O_2 following a 14-day incubation. However, MoS_2 was still detectable using Raman spectroscopy with the added benefit of observing changes in the spectral profile. This method not only demonstrates that submicron plates can be detected with Raman micro-spectroscopy but highlights the sensitivity and advantage of using Raman for monitoring plate integrity and/or degradation inside a cell.
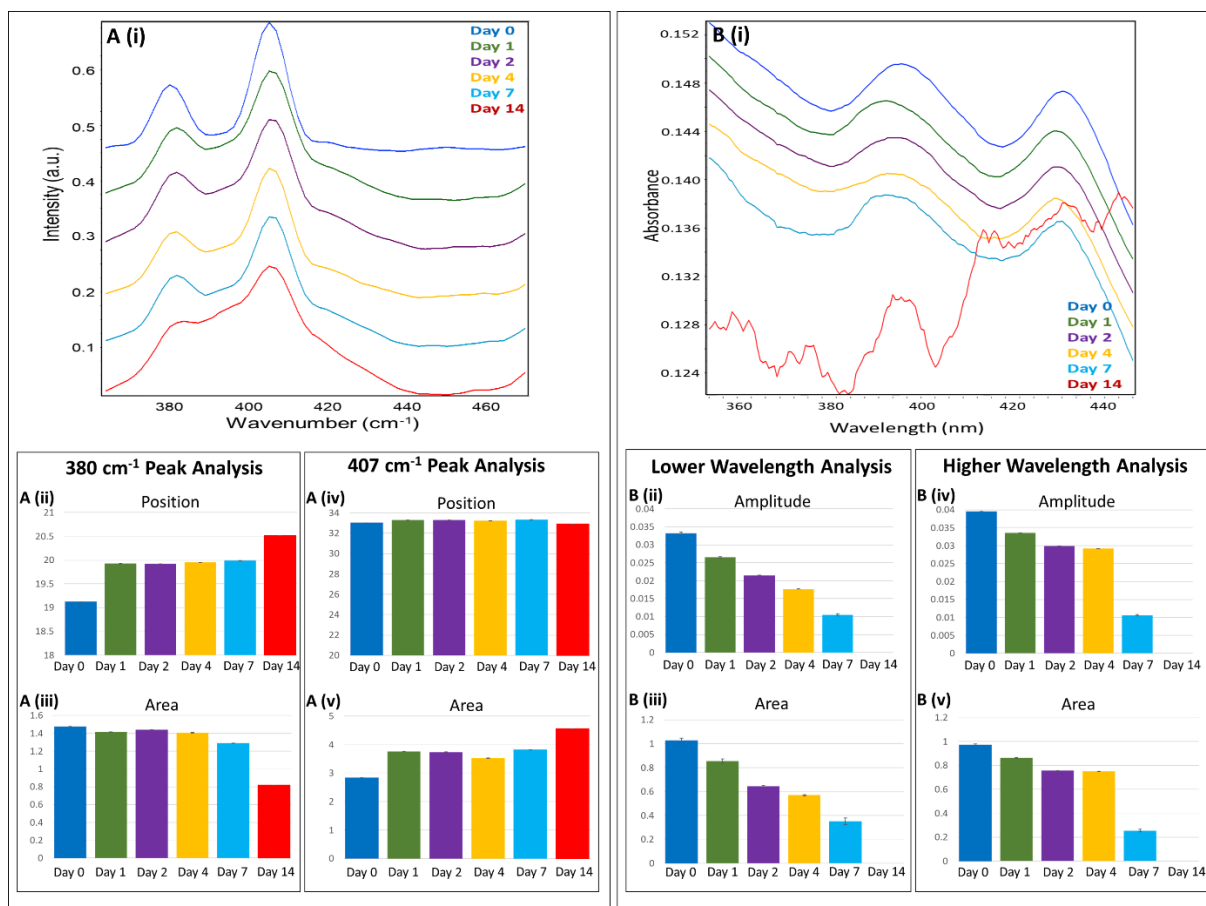
Figure 1 Raman analysis of 105 nm MoS_2 degraded over time (0, 1,2,4,7, and 14 days) using H_2O_2 at a concentration of 2000 μM Figure 1A(i) Raman spectra from 365 to 470 cm^{-1}. Figure 1A(ii-iii) Gaussian-Lorentzian curve position and area analysis of 380 cm^{-1} Raman peak. Figure 1A(iv-v) Gaussian-Lorentzian curve position and area analysis of 407 cm^{-1} Raman peak. Figure 1B(i) UV-Vis absorbance spectra from 550 to 700 nm. Figure 1B(ii-iii) Gaussian-Lorentzian curve amplitude and area analysis of the lower wavelength peak. Figure 1B(iv-v) Gaussian-Lorentzian curve amplitude and area analysis of the higher wavelength peak. Figure A-B(i) Spectra are off-set for clarity.

Methodology used for Raman map analysis

Raman spectroscopy has been shown to be suitable for detecting subtle changes in the integrity of the MoS_2 and therefore it was now employed to explore the integrity of the MoS_2 within the cell micro-environments. Figure 2 is a schematic representation of the methodology used for the analysis of selected macrophage-like THP-1 cells, exposed for 4 h to MoS_2 and incubated for a subsequent 24 h in medium. Figure 2A is a bright-field image depicting the grid from where the spectral mapping has been acquired. Transmission electron microscopy (TEM) was previously performed(34) and indicated MoS_2 was internalised inside single membrane vesicles within the cell following a short time-point of 4 h, and therefore the Raman map included parts of the nucleus, cytoplasm, perinuclear region and vesicles, to cover all aspects of the cell. Figure 2B is a representative spectrum from 365-1800 cm^{-1}, revealing the

contributions of both MoS$_2$ material (red) and biological (blue) information within the same spectrum. A 2D image showing the identification/location of MoS$_2$, following multivariate FA and CLS fitting, can be seen in Figure 2C (i), along with the corresponding spectra in the range of 365-470cm^{-1} (Figure 2C(ii)). Similarly, an image showing the location of different biological regions can be seen in Figure 2D (i), along with the corresponding spectra in the range of 800-1800cm^{-1} (Figure 2C(ii)), the features of which can be assigned to specific modes of different biochemical species(43). This demonstrates the ability to examine two aspects, (i) the distribution and integrity of the MoS$_2$ in the cell as a function of exposure time and (ii) the characteristics of the micro-environment of the MoS$_2$ plates in the cell. The details of these analyses will be elaborated further.
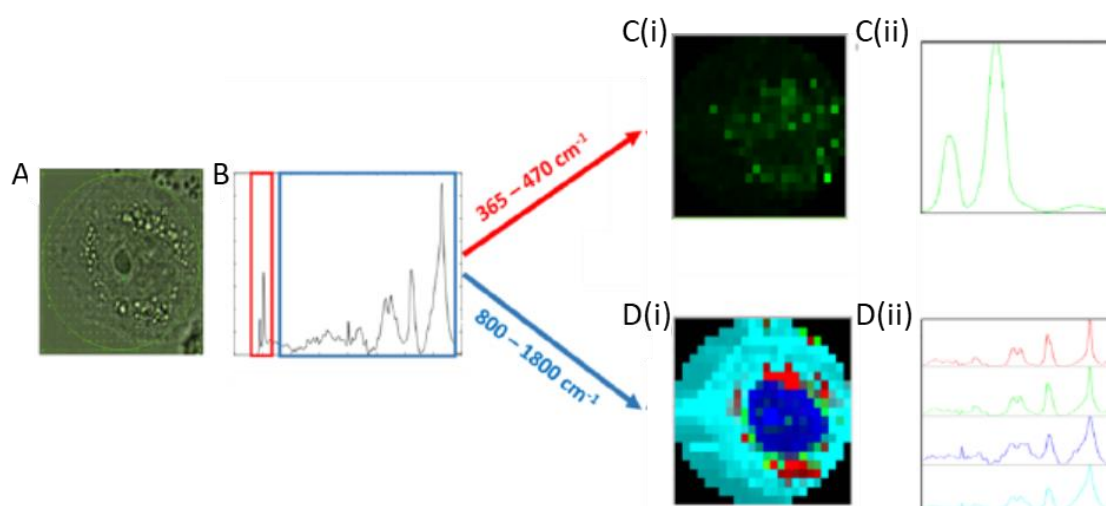

Figure 2 Analysis of Raman Map of a macrophage-like THP-1 cell following a 24 h incubation. Figure 2A bright field image of THP-1 cell under x100 water immersion and taken on a Horiba dual Raman microscope. Figure 2B Spectra in the range of 365 -1800cm^{-1}in which MoS$_2$ material and fingerprint regions are indicated by red and blue overlay boxes, respectively. Figure 2C (i) cluster location of MoS$_2$ material inside the cell along with corresponding spectra in the range 365 – 470 cm^{-1} (Figure 2C(ii)). Figure 2D (i) image overlay showing the location of four biomolecules in the fingerprint region in the cell along with corresponding spectra in the range 800-1800 cm^{-1}(Figure 2D(ii)).

Detection and characterisation of MoS$_2$ in-vitro over time

The first step is to monitor the integrity of the material inside the cell and detect any changes or alterations to the MoS$_2$ plates following incubation (4, 24 or 72 h) in the cellular micro-environment. The Raman map, in Figure 3, of a cell incubated for 4 h following exposure, was analysed using only the spectral range from 365–470 cm^{-1}, which contains the

strongest MoS_2 peaks at 380 and 407 cm^{-1}. An unsupervised, multivariate FA approach, available in the instrument (Labspec 5) software, was applied to identify clusters with molecular/spectral differences based on Raman spectra. Following the identification of Factors, supervised CLS analysis was then preformed to produce pseudo-colour images illustrating the distribution of each Factor within the Raman map. Figure 3A is a bright-field image depicting the grid from where the spectral mapping has been acquired. MoS_2 is observed to be present in large quantities throughout the cell, widely distributed in various locations, indicative of the early uptake and processing of the MoS_2 by the immune cell. Following application of the FA algorithm, three different Factors are identified, the distributions of which are shown in the 2D image overlay of Figure 3B. The distribution and/or location of each of the three Factors is displayed separately in 3D format in Figure 3C-E (i). Factor 2 is dispersed more diffusely over the cell, while Factor 1 and 3 are more confined to discrete areas within the cell. Examining the spectra (Figure 3C-E (ii)), no major differences in MoS_2 material are apparent, although a slight change in ratio between E^1_{2g} and A_{1g} modes can be seen. Also, a minor red shift of both peaks can be seen in Factor 2 and 3. ACS Material LLC[44] have reported a similar red shift of both peaks with their Bio-MoS_2 samples (MoS_2 in the presence of Bovine Serum Albumin), suggesting a biological interaction of MoS_2 with proteins following a 4 h incubation (Factor 2 and 3) but no indication of degradation.
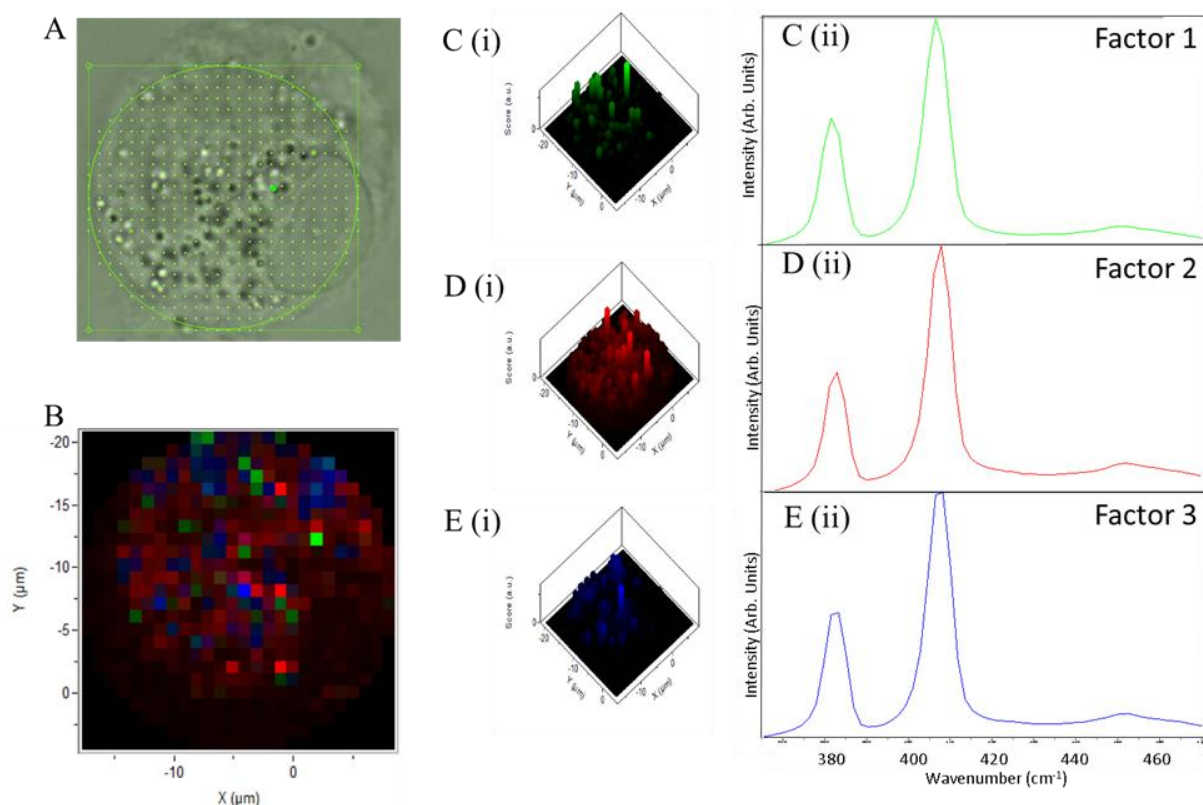
Figure 3 Raman Map Analysis of a macrophage-like THP-1 cell following a 4 h incubation. Spectral range 365 to 470 cm^{-1}. Figure 3A bright field image of THP-1 cell under x100 water immersion and taken on a Horiba dual Raman microscope. Figure 3B 2D overlay image of the Raman map showing the location of the three Factors (Factor 1 – green, Factor 2 – red, Factor 3 – blue). Figure 3C (i) 3D construction showing the location of Factor 1 within the cell. Figure 3C (ii) mean spectra of Factor 1 displayed. Figure 3D (i) 3D construction showing the location of Factor 2 within the cell. Figure 3D (ii) mean spectra of Factor 2 displayed. Figure 3E (i) 3D construction showing the location of Factor 3 within the cell. Figure 3E (ii) mean spectra of Factor 3 displayed.

24 h after the 4 h exposure to MoS$_2$, the cellular Raman map of Figure 4 was also analysed using the FA algorithm, within the spectral range from 365–470 cm^{-1}. Factor 1 has a spectrum similar to the original MoS$_2$ used for exposure, while, in contrast, Factor 2 (red) shows a significant decrease in strength and a minor red shift of the E$^1_{2g}$ mode, as well as a broadening of the A$_{1g}$ mode. The distribution of Factor 2 appears predominantly in the perinuclear area of the cell. Factor 3 also shows a decrease in intensity of the E$^1_{2g}$ mode, a shift to higher wavenumber and a broadening of the 407 cm^{-1} peak, although to a lesser extent than that observed in Factor 2. The spectral profiles of MoS$_2$ plates found in Factor 2/3 match the Raman spectral characteristics of degraded MoS$_2$ found in Figure 1A. Notably, micro/nano plates stabilised in sodium cholate surfactant are sensitive to alterations in salt concentration. Plates stabilised in sodium cholate surfactant are, however, prone to agglomeration, dependent on the salt concentration. Therefore, induced agglomeration of submicron plates was carried

out by incubating MoS_2 in varying concentration of sodium chloride (40, 20, 10 and 5 mg/ml). The Raman spectra from induced agglomeration can be seen in Supplemental Figure 6, in which no spectral changes could be observed. Therefore, it can be concluded that any spectral changes observed of MoS_2 in-vitro are not due to plate agglomeration. Consequently, it can be stated that, following a 24 h incubation of MoS_2 inside macrophage-like cells, significant degradation of MoS_2 occurs. Macrophages aid in the digestion of pathogens/materials following phagocytosis, and it has been reported that macrophages have the ability to produce superoxide radicals through two enzymatic systems (NADPH oxidase and NO synthase) to degrade carbonaceous nanoparticles[45]. After 24 h, the distribution of MoS_2 is concentrated in discrete regions of the cell when compared to the distribution of the MoS_2 following 4 h incubation. Understanding the plate distribution and the corresponding cellular processing of these foreign substances will hold a key to understanding how the MoS_2 is degraded.
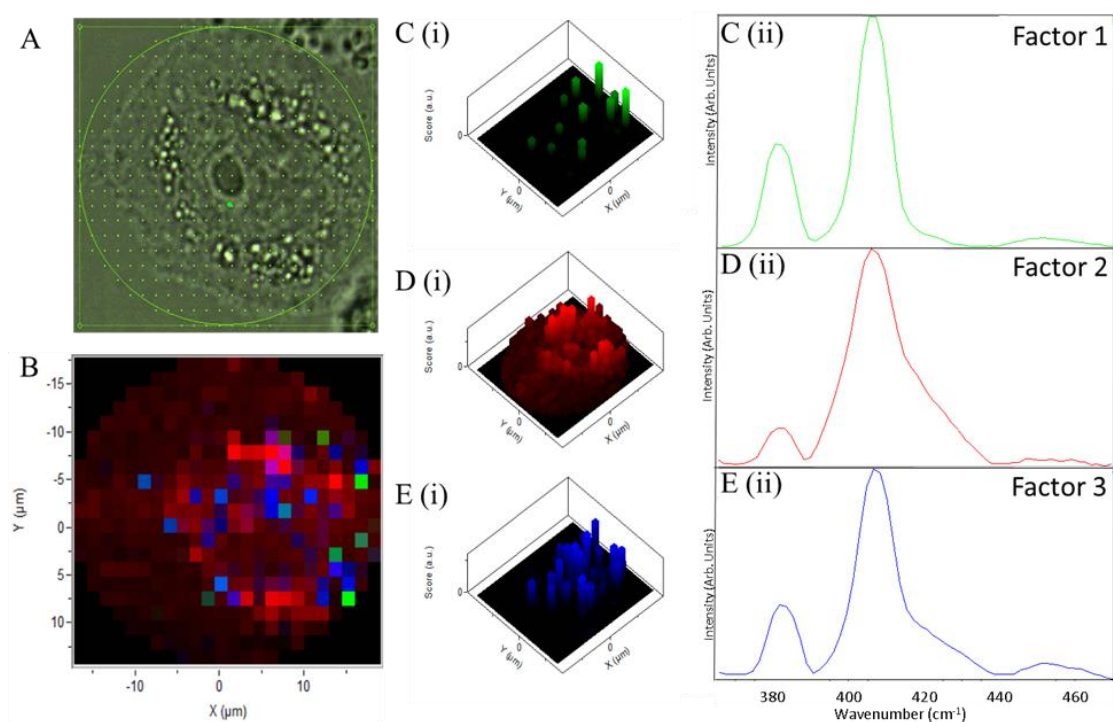

Figure 4 Raman Map Analysis of a macrophage-like THP-1 cell following a 24 h incubation. Spectral range 365 to 470 cm^{-1}. Figure 4A bright field image of THP-1 cell under x100 water immersion and taken on a Horiba dual Raman microscope. Figure 4B 2D overlay image of the Raman map showing the location of the three Factors (Factor 1 – green, Factor 2 – red, Factor 3 – blue). Figure 4C (i) 3D construction showing the location of Factor 1 within the cell. Figure 4C(ii) mean spectra of Factor 1 displayed. Figure 4D (i) 3D construction showing the location of Factor 2 within the cell. Figure 4D(ii) mean spectra of Factor 2 displayed. Figure 4E (i) 3D construction showing the location of Factor 3 within the cell. Figure 4E(ii) mean spectra of Factor 3 displayed.

The Raman map in Figure 5, of a cell incubated for 72 h following 4h exposure, was similarly analysed over the spectral range from 365–470 cm^{-1}. Similar to the 4h incubation (Figure 3), MoS_2 is seen to be present in large quantities throughout the cell, Factor 2 showing a broad distribution with varying intensities all over the cell. Factor 1 and 3 from 72 h analysis shown in Figure 5 (C and E) are more confined to selected areas than any Factors observed in either the distributions of the 4 or 24 h time-points. An evident increase in concentration to a localised area is also indicated, following a 72 h incubation post-exposure. Examining the spectra (Figure 5C-E (ii)), no significant degradation in MoS_2 material is apparent, although a slight change in ratio between E^1_{2g} and A_{1g} modes can be seen. Also, a minor red shift of both peaks can be seen in Factor 2 and 3. Therefore, it can be concluded that no degraded material remains inside the cell or can be detected following an incubation in a cellular micro-environment for 72 h.
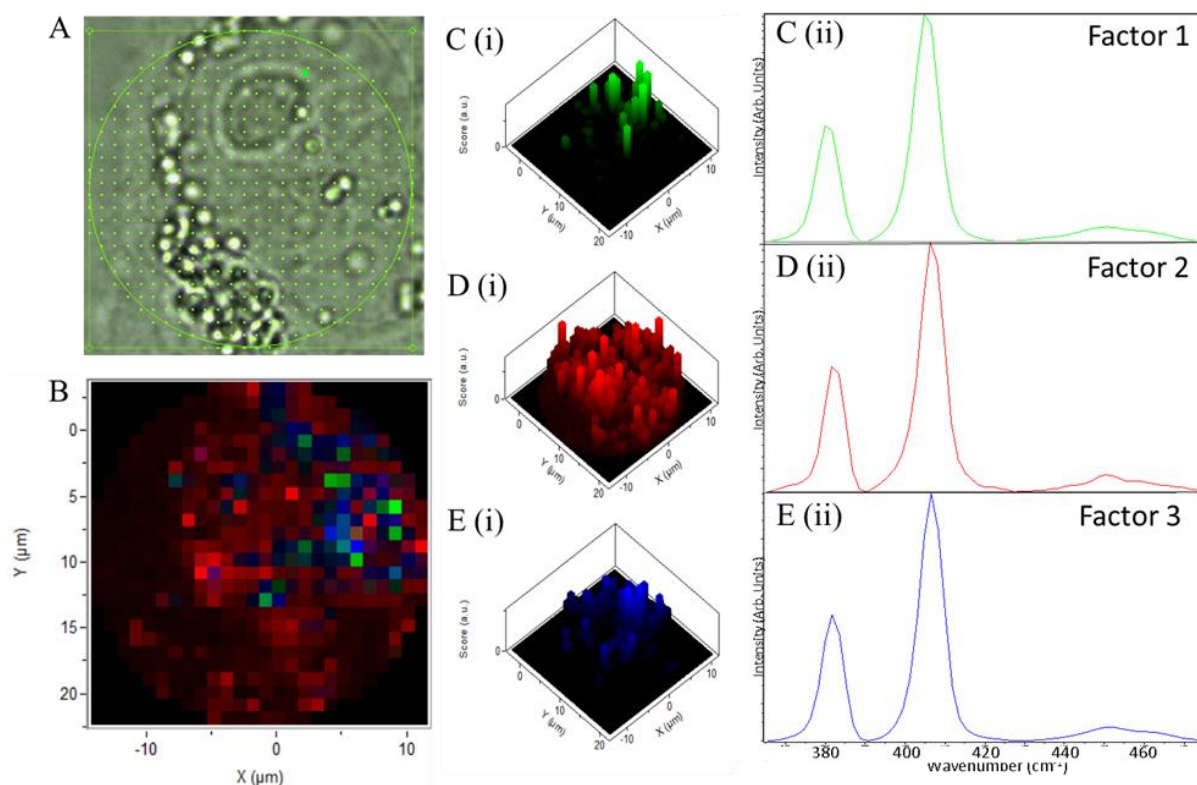

Figure 5 Raman Map Analysis of a macrophage-like THP-1 cell following a 72 h incubation. Spectral range 365 to 470 cm^{-1}. Figure 5A bright field image of THP-1 cell under x100 water immersion and taken on a Horiba dual Raman microscope. Figure 5B 2D overlay image of the Raman map showing the location of the three Factors (Factor 1 – green, Factor 2 – red, Factor 3 – blue). Figure 5C (i) 3D construction showing the location of Factor 1 within the cell. Figure 5C(ii) mean spectra of Factor 1 displayed. Figure 5D (i) 3D construction showing the location of Factor 2 within the cell. Figure 5D(ii) mean spectra of Factor 2 displayed. Figure 5E (i) 3D construction showing the location of Factor 3 within the cell. Figure 5E(ii) mean spectra of Factor 3 displayed.

Notably, the Raman maps at different time points from Figure 3-5 were recorded on different cells and were analysed independently. A clear time progression is therefore not easily depicted, or quantifiable. A representative figure, illustrating the 2D images over time, can also be seen in supplemental (Supplemental Figure 7).

Investigating the cellular micro-environments in which MoS$_2$ is encompassed

Degradation of MoS$_2$ at 24 h following internalisation has been observed, and thus the next step is to profile the cellular micro-environment in which it is localised. The Raman map of Figure 4 was examined in the spectral range of 365-1800cm^{-1}, in which the main MoS$_2$ and cellular peaks are located, by similarly applying the FA algorithm followed by supervised CLS analysis (Figure 6). When FA is explored in this range, the dataset was classified into four factors based on different spectral features contributing from both MoS$_2$ plates and cellular features. All components show the presence of MoS$_2$ material in varying concentrations. This confirms the uptake of MoS$_2$ inside the cells along with the cellular micro-environment in which it is surrounded by. In contrast to the 4 h incubation, after which a diffuse distribution of material could be seen throughout the entire cell, observations after a longer incubation period of 24 h show the migration of MoS$_2$ towards the perinuclear region (Factor 1, Figure 6C). Vesicles associated with Factor 2 (Figure 6D (i)) are located in the area surrounding the nucleus of the cell, similar observations were also seen for the 4 and 72 h incubations (Supplemental Figure 2 and 4). Vesicles related to both the endocytic and exocytic systems are commonly found in this "perinuclear cloud", including but not limited to endosomes, lysosomes, and Golgi originated vesicles(46). Vesicles present within the "perinuclear cloud" exhibit reduced motility, although a small portion will be transported through the cytoplasm to the peripheral of the cell for exocytosis(46).

As the plates were observed to degrade following a 24 h incubation inside macrophage-like cells, smaller quantities of MoS$_2$ could be detected in Factor 2, 3 and 4 when compared to Factor 1. A more uniform concentration of plates could be observed in macrophage-like cells incubated for both 4 (Supplemental Figure 2) and 72 h (Supplemental Figure 4) with MoS$_2$. When comparing the distribution of Factors to the bright-field image, it appears that Factor 1 and 4 are cytoplasmic in origin. Factor 2 has a direct correlation with vesicles present in the "perinuclear cloud" and Factor 3 appears consistent with the location of the nucleus. Therefore,

when comparing the spectral maps from Figure 4 and 8, it can be concluded that Factor 1 (Figure 6) contains non-degraded MoS_2 while Factors 2, 3 and 4 contain degraded MoS_2, although to a lesser extent in Factor 3 and 4. Notably, it may appear that MoS_2 is detected inside the nucleus, although this is not the case. The spectra are acquired through (numerical aperture 0.90) multiple planes of the cell and MoS_2 may be present above/below the nucleus, but not inside and for this reason the nuclear data (Factor 3) was not included in analysis.
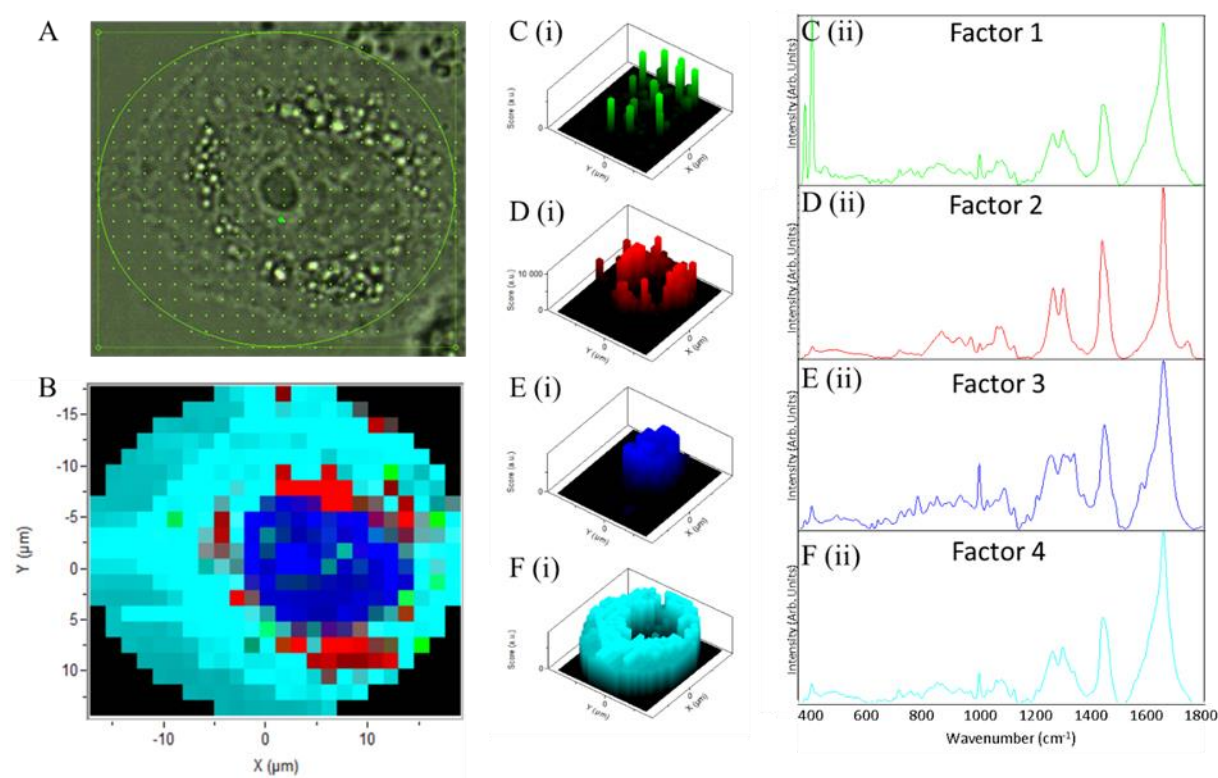

Figure 6 Raman Map Analysis of a macrophage-like THP-1 cell following a 24 h incubation. Figure 6A bright field image of THP-1 cell under x100 water immersion and taken on a Horiba dual Raman microscope. Figure 6B 2D overlay image of the Raman map showing the location of the four Factors (Factor 1 – green, Factor 2 – red, Factor 3 – blue, Factor 4 – cyan)). Figure 6C (i) 3D construction showing the location of Factor 1 within the cell. Figure 6C(ii) corresponding spectra of Factor 1 displayed. Figure 6D (i) 3D construction showing the location of Factor 2 within the cell. Figure 6D(ii) corresponding spectra of Factor 2 displayed. Figure 6E (i) 3D construction showing the location of Factor 3 within the cell. Figure 6E(ii) corresponding spectra of Factor 3 displayed. Figure 6F (i) 3D construction showing the location of Factor 4 within the cell. Figure 6F(ii) corresponding spectra of Factor 4 displayed.

Principal component analysis (PCA) is a size reduction tool used in data processing to discriminate different samples or cell locations according to the differences in biochemical composition. The spectral features discriminating the two or more data sets is then displayed as a principal component (PC), PC1 normally showing the highest degree of variability in the data set. PCA of the pixels grouped according to the FA was carried out over the range of 800-1800 cm^{-1}, to compare the micro-environment in which MoS_2 is internalized after 24 h

incubation. PCA was carried out to compare Factor 1 and Factor 2, as shown in the scatter plot in Figure 7A (i), in which Factor 1 (green) is clearly differentiated from Factor 2 (red) based on PC1. The loadings for PC1 are displayed in Figure 7A(ii), which shows Factor 1 contains protein (phenylalanine – 1003, 1208, 1578 and 1617 cm^{-1} and Amide III – 1233 cm^{-1}) and nucleic acids (1340, 1480 and 1578 cm^{-1}). Interestingly, bands present at 1578, 1615 and 1679 cm^{-1} (Factor 1), which can be assigned to bound and free NADH (Nicotinamide adenine dinucleotide),(47) could be observed, which was not the case for the 4 and 72 h time-points (Supplemental Figure 3 and 5). The prominence of NADH signatures is consistent with the need for additional energy from the cell to undertake the degradation process. Factor 2 is dominated by positive peaks with a high concentration of lipids (1066-1080, 1266, 1301, 1440, 1659 and 1749 cm^{-1}) present along with carbohydrates (868 cm^{-1}).

Clear separation based on PC1 can be observed for Factor 2 (red) versus Factor 4 (cyan), the separating components matching the loadings for Factor 1 versus Factor 2 (Figure 7B(i)). This suggests that Factor 1 and Factor 4 have a similar biochemical composition in the range 800-1800 cm^{-1} and this is confirmed by PCA analysis (Figure 7C(i)), by which no separation is achieved. Considering the full range of Factor 1 and Factor 4 displayed in Figure 6, the only difference between these components is the presence of relatively larger quantities of non-degraded MoS_2 in Factor 1, compared to minor quantities of degraded material in Factor 4. Plate degradation was not detected in macrophage-like cells following a 4 or 72 h incubation. However, PCA analysis was also carried out and can be seen in supplemental (4 h - Supplemental Figure 3, 72 h - Supplemental Figure 5).
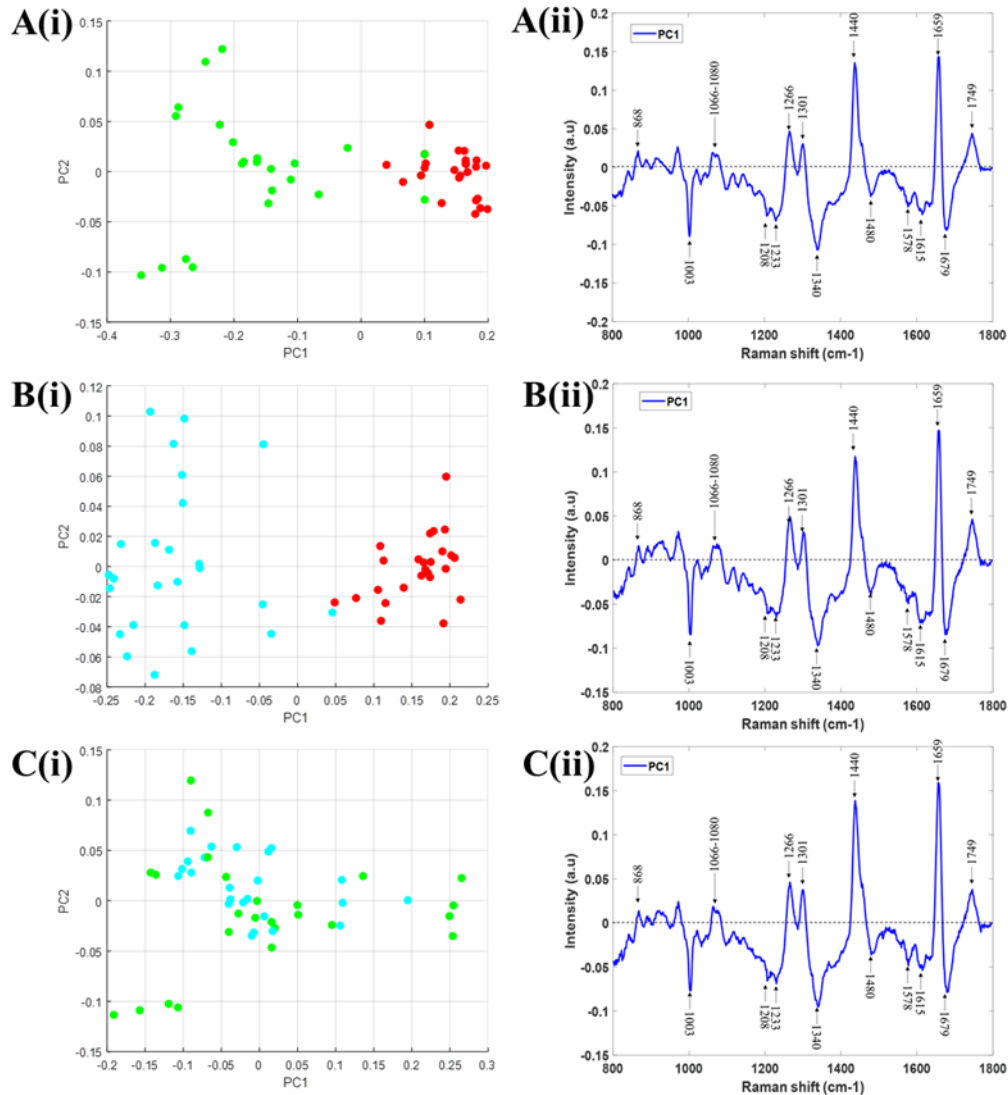
Figure 7 Principal components analysis to observe differences in the Factors observed in Raman Maps following 24h incubation. Figure 7A(i) PCA scatter plot of Raman spectra from Factor 1 (green) and Factor 2(red), plotted PC1 versus PC2. Figure 7A(ii) PC1 loadings showing the separation between the two Factors. Figure 7B(i) PCA scatter plot of Raman spectra from Factor 2(red) and Factor 4(cyan), plotted PC1 versus PC2. Figure 7B(ii) PC1 loadings for Factor 2 versus Factor 4. Figure 7C(i) PCA scatter plot of Raman spectra from Factor 1(green) and Factor 4(cyan), plotted PC1 versus PC2. Figure 7C(ii) PC1 loadings for Factor 1 versus Factor 4.

Identification of cellular micro-environments

Based on the PCA, Factor 2 appears the most lipidic in nature, while Factors 1 and 4 are relatively protein rich in composition. The PCA loading was then compared with an in-house data set of 82 pure biological macromolecule components, including proteins, lipids, enzymes etc. These cellular component standards were then used to identify potential constituent compounds which contribute to the differentiation of the sub-cellular environments. Two components are compared in parallel by subtracting one component from the other to

create a difference spectrum, which is then compared against the PCA loadings (Figure 8C). From all the components tested, Factor 2 showed a spectral profile consistent with the prominence of phosphoglycerides (PG), that contain an acyl group derived from a phosphatidic acid, alternatively called the phosphatidyl family (Figure 8D)(48). Phosphatidyl lipids are composed of a lipid backbone, two fatty acids chains and one phosphoric acid group esterified to a head group (e.g. serine, choline, ethanolamine etc.)(48), and are commonly detected in cell membranes. A quantitative profile of macrophage PG has shown that an increase in phosphatidylcholine (PC) and phosphatidylethanolamine (PE) are expected following differentiation of monocytes into macrophages(49). In another study by Meijuan Cheng *et al*, it was shown that PC had anti-inflammatory effects following lipopolysaccharide (LPS) exposure by reducing the level of (tumour necrosis factor) TNF-α secretion(50). Factor 1 and 4 were also compared with the in-house dataset and a high degree of similarity with lysozyme was observed (Figure 8D). Lysozyme is an enzyme found in granulocyte immune cells (e.g. neutrophils and macrophages) in which the cytoplasm contains multiple azurophilic/lysosomal granules containing digestive enzymes as a first line of defense(51). Formerly known as muramidase, lysozyme permeabilises the bacterial cell membrane by the hydrolysis of the peptidoglycan within the cell wall(52). The presence of lysozyme within the micro-environments described by Factors 1 and 4 may aid in the degradation of the MoS_2 due to its anti-microbial abilities.
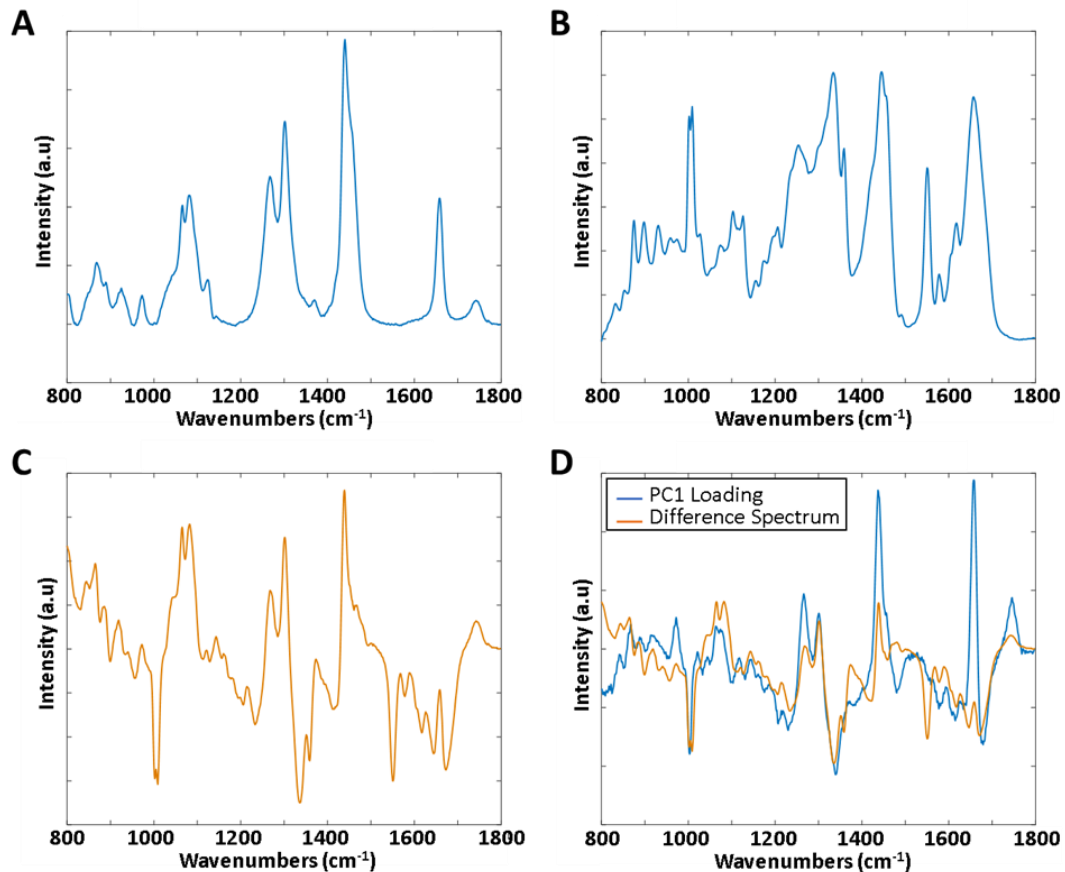
Figure 8 Analysis of components present in PCA loadings. A Phosphatidyl family lipid standard. B Lysozyme enzyme standard. C Difference spectrum (Lysozyme minus phosphatidyl lipid). D Comparison of PC1 loading from Factor 1 versus Factor 2 (blue) against the difference spectrum (orange).

Detection of neutral lipids following exposure to MoS₂

Raman maps from all time points indicate that the macrophage-like cells, in response to the uptake of foreign material, express a certain amount of lipids forming vesicles surrounding the perinuclear region (Factor 2, 4 h - Supplemental Figure 2, 24 h – Figure 6 and 72 h -Supplemental Figure 4). In order to confirm the presence of neutral lipids within the cytoplasm, the cells were stained with Oil Red O. Neutral lipids are uncharged and hydrophobic in nature and are commonly surrounded by a phospholipid monolayer in macrophages to form lipid bodies (LBs)(53). Untreated cells will contain LBs within the cytoplasm of THP-1 cells, that have been differentiated into macrophages using phorbol 12-myristate 13-acetate (PMA)(54), and this can be seen in Figure 9 (negative treatment - NT). Neutral lipids are represented by the orange/red colour inside the cells. When comparing the 4 h incubation to the untreated cells, there is a visible increase in the number of lipids present. Lipid metabolism can be different between classically activated (M1) and alternatively activated macrophages

(M2), but it has also been shown that an increase in phosphatidylcholine and phosphatidylethanolamine is expected during macrophage differentiation (49,55). Macrophages are known to secrete cytokines and proteins, one of which is lipoprotein lipase (LPL), which is known to increase the level of lipids accumulated intracellularly(56). An increase in TNF-α in THP-1 cells exposed to industrial grade MoS_2 has previously been shown(34), although White *et al*. have shown this will not affect LPL levels(56). Interestingly, the 24 h incubation not only has a further increase in internal lipids, but external lipids excreted by the cells can also be observed, as indicated by blue arrows in Figure 9. This further indicates the need for increased cellular energy, as indicated by the increased levels of NADH. When cells have been incubated with MoS_2 for 72 h there is a reduction in the quantity of Oil red O stain detected inside the cell. This reduction and the fact that MoS_2 degradation was not detected in cells incubated for 72 h, suggest that cells have halted the production and storage of neutral lipids and/or digestive enzymes, as the foreign threat has been eliminated. It has been suggested that the interaction of LBs with phagosomes may play two roles:1-as a pathogen-driven process by which the pathogen uses the host lipid supply to improve the chances of infection, or 2-that LBs target phagosomes containing pathogens as way to eliminate the foreign threat(57).
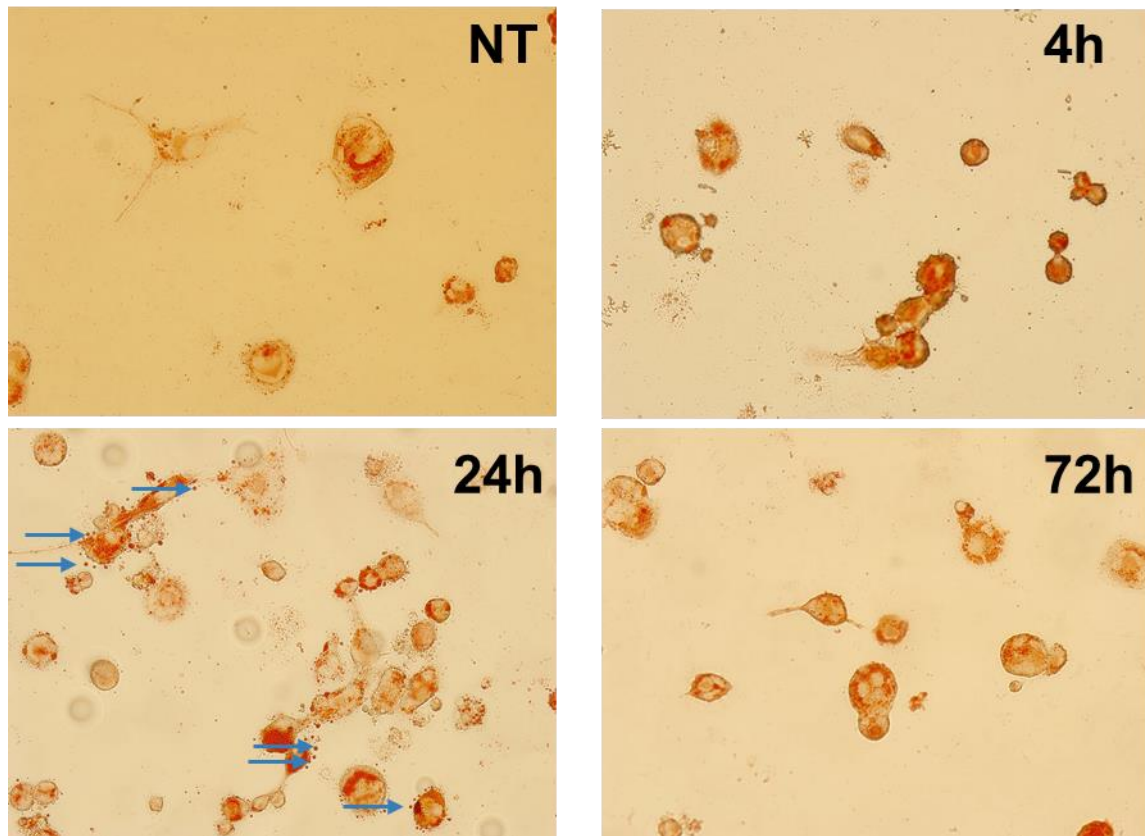
Figure 9 Identification of neutral lipids in macrophage-like THP-1 cells following a 4, 24 or 72 h incubation with MoS_2. NT are untreated control cells grown in supplemented media following PMA activation. Lipid are stained using Oil Red O. Extracellular lipids can be seen in 24 h incubation and are indicated by blue arrows.

Discussion

Determining the presence of nanomaterial and/or submicron plate degradation *in-vitro* is of paramount importance as non-degraded material can cause a reduction in clearance, prolonged retention and ultimately can lead to accumulation of material within vital organs (58). For the safe use of MoS_2 in biomedical applications the dissolution within biological environments needs to be fully understood. It is well documented that the size, shape and surface area of both nano and submicrometric material can affect the fate, transport and recognition of materials by the immune system and therefore material degradation. When MoS_2 are oxidized in the presence of H_2O_2 it causes the generation of soluble molybdenum species due to etching of the plate edges. The material used in this study contained a high level of endotoxin suspected of being bound to the particulate edge. In order to mimic the possible cellular degradation of MoS_2 (19), the MoS_2 (100 μg/ml) was incubated ex-vivo with relatively high concentrations of H_2O_2 (Figure 1 – 2000 μM) oxidizing agent to induce degradation of

plate samples. H_2O_2 is commonly found in phagocytic immune cells such as macrophages and neutrophils although at lower concentrations of 50-100 μM(59). Z, Wang *et al* have shown MoS_2 dissolution of chemically exfoliated sheets is greatly associated with pH and additional cell culture components showed lower rates of dissolution (60). Additionally, they reported multi-layer sheets prepared by ultrasonically exfoliation showed slower rates of degradation. When MoS_2 sheets were incubated in H_2O_2 concentrations well above biologically relevant levels to induce degradation ex-vivo, a relatively slow rate of degradation was achieved, with particulate material still detected following 14 days incubation. Samples from each time-point were analysed by both Raman micro-spectroscopy and UV-Vis absorption spectroscopy, demonstrating Raman to be more effective with a lower limit of detection. Furthermore, alterations in spectral profile could be observed with Raman spectroscopy showing a decrease in intensity for the E^1_{2g} Raman mode (380 cm^{-1}) while peak broaden and/or increase in peak area could be observed for the A_{1g} mode (407 cm^{-1}). Additionally, it can be noted that any alterations in spectral profile compared to the pristine MoS_2 samples is not due to aggregation as can be seen in supplemental figure 6. These findings provided evidence to aid in interpretation and characterization of Raman findings when investigating MoS_2 in-vitro within human macrophage-like cells.

Following analysis of Raman maps in the spectral range of 365 -1800 cm^{-1}, it was observed that MoS_2 is taken up by the cells and the biochemical composition of the surrounding micro-environment was characterised. The MoS_2 location appears more diffuse following a 4 h incubation, indicating the early uptake of the material, most likely internalised in phagosomes and the initiation of the cellular reaction to a foreign substance in its environment. Following a 24 h incubation, high levels of MoS_2 were detected, but seen to be more localised to discrete regions of the cell, for further processing or possible binding with lysosomes to form phagolysosomes. Although phagosome to phagolysosome is the most probable uptake pathway when considering macrophages, the non-phagocytic uptake mechanisms should not be ignored, as cells function in a multi-disciplinary way. When cells have interacted with the plate for 72 h (Supplemental Figure 4), a more diffuse location of non-degraded MoS_2 was detected throughout the cell similar to observations at 4 h time points (Supplemental Figure 2). Traditionally, degradation would be expected in a lysosomal environment, although samples used throughout this study are industrial grade and contain high levels of LPS. LPS has been

known to reduce the enzymatic activity of lysozyme(61), potentially explaining why both degraded and non-degraded MoS_2 could be detected within macrophage-like cells.

Particulate material uptake can be influenced by a range of characteristics that include size, shape or charge, although cell type along with their biological function can greatly affected the fate of the material. Passive, non-specific uptake(62,63) is well known, although macrophages play a crucial role in active uptake as the first line of defense in the immune system when invaded by a foreign threat. Therefore, the common uptake mechanism for macrophages is initiated by phagocytosis to form a phagosome, which later binds with a lysosome to form a phagolysosome to destroy/degrade the foreign material with the aid of digestive enzymes. Non-phagocytic pathways are also considered when examining the uptake in macrophages and can include clathrin coated vesicles, caveolae vesicle or micropinocytosis (12). The initial uptake mechanism may differ slightly for each pathway, although Zhu *et al.* have shown that the vesicles from all pathways of uptake of MoS_2 within cancer cells are destined to accumulate in lysosomes (12).

In the current study, non-degraded MoS_2 was detected in macrophage-like cells following a 4 h incubation with plates, illustrating the early uptake mechanism. Particulate material may be internalised within phagosomes, early/late endosomes, clathrin or caveloae vesicles. Following a prolonged *in-vitro* incubation of 24 h, degraded MoS_2 plates are detected. Accelerated degradation could be due to the primary vesicle containing internalised material, fusing with an acidic lysosome, the change in pH causing the dissolution of the MoS_2 plates. Consistent with the observations of Wang *et al.*, no degradation of MoS_2 following a 72 h incubation was observed (12). This could be due to a slower uptake mechanism or MoS_2 is within non-lysosomal compartments, as a result of which the cell has exhausted its resources and is recovering to produce more lysosomes, or it is preparing for exocytosis of a material.

It is well known that both smooth and rough endoplasmic reticulum (ER) are in close proximity to the nucleus(64), which correlates with the distribution of Factor 2 observed following a 24 h incubation time-point. Additionally, the accumulation of neutral lipids is commonly associated with the lumen of the ER in which budding of the ER membrane allows

the formation of LBs(65). LBs are frequently identified in the cytoplasm of foam cell macrophages as a mechanism to defeat infection(66) and are more recently described as inflammatory organelles(67). Furthermore, enzymes involved in carbohydrate metabolism, fatty acid synthesis and lipid metabolism are all associated with LBs(66). Additionally, LBs contain a hydrophobic core surrounded by a phospholipid monolayer which further connects with the identification of the phosphatidyl membrane lipids in Factor 2 (Figure 8).

The production of industrial grade MoS_2 materials used in this study is carried out in a non-sterile environment in which the possibility of contamination from endotoxin (also known as LPS), is certain. Previously, particulate MoS_2 of three lateral sizes (50, 117 and 177 nm) prepared by the same production method have contained high levels of endotoxin with a direct increase in LPS with increasing surface area(34). LPS is commonly found on the outer cell membrane of gram-negative bacteria and is composed of three main components: the O antigen, the core and a Lipid A moiety(61). The O antigen is found on the outer most region on the molecule and can vary between species while the Lipid A moiety is known to cause the most toxicity and is responsible for immune responses(68). Two common forms of macrophages are called M1 and M2 respectively(69). M1 macrophages are classically activated by exposure to LPS or interferon-gamma (IFN-γ), while M2 macrophages are alternatively activated by exposure to cytokines such as IL-4 or IL-13(70), through the interaction/binding with toll-like receptors(71) on the cell surface which leads to accumulation of triglycerides (neutral lipid) along with the decrease in lipolysis and increase in the uptake of free fatty acids from their environment(72,73). Over a time period of 24 h, macrophage activation can increase in a dose dependent manner due to the presence of LPS(74). A range of cytokines are commonly excreted by macrophages in response to LPS exposure, including but not limited to, TNF-α, interleukin 1-β (IL-1beta) and IL-6(74), which in turn are interconnected with a range of cascade pathways(9). Therefore, the presence of LPS on the surface of these industrial grade particulate materials will greatly contribute to the cellular response and the destiny of the material once phagocytosed. Interestingly, non-degraded MoS_2 was detected in an enzymatic micro-environment (Factor 1 - Figure 6) with spectral profiles similar to lysozyme (Figure 8D). As reported previously by Lukasiewicz J *et al*., LPS has the ability to reduce the activity level of lysozyme and therefore aids in understanding why both degraded and non-degraded MoS_2 could be detected in macrophage-like cells following exposure (61).

NADH is detected using Raman micro-spectroscopy in macrophage-like cells following a 24 h incubation with MoS_2. This demonstrates the need for cellular respiration by the cell and suggests that the cell is carrying out additional processes of cellular response. The cellular micro-environment for both 4 and 72 h incubation with MoS_2 (Supplemental Figure 3 and 5) was also analysed using PCA and no signatures of NADH could be detected. Shabany *et al*. have shown NAD+ is directly related to TNF-α production following exposure of pro-inflammatory macrophages to LPS (75). As previously reported(34), the plates used in these studies are industrial grade and contain LPS contaminates which have been shown to stimulate macrophages to secrete TNF-α in a size dependent response with the smallest particles eliciting the highest reactivity. The production of LBs could also be responsible for the increased levels of NADH at the 24 h time-point, as the Oil Red O staining indicates that there is a saturation of LBs following a 24 h incubation. As NADH is not detected in cells following a 4 h incubation (Supplemental Figure 3), it would suggest the initiation of a cellular reaction in response to a foreign threat occurs post 4 h incubation with MoS_2. As a decrease in LBs is observed following a prolonged incubation of 72 h, along with no incidence of NADH (Supplemental Figure 5), this would suggest the cell has exhausted its energy supply post 24 h and reduced/ceased the production of LBs. Subsequent to LBs formation in bone marrow-derived macrophages (BMDM), Santucci *et al*. have reported a similar decrease in LBs content when cultured without exposure to a foreign threat whereas infected BMDM exhibited a reduction in lipid degradation (76).

Due to the fixation process prior to Raman spectroscopic analysis, a separate sample must be prepared for each incubation time-point and, as a result, a different cell and/or interaction was interrogated for each time-point although a figure illustrating the 2D images from each cell over time can be seen in supplemental figure 7. Notably, the rate of internalisation and/or quantity of material internalised can vary from cell-to-cell and within each sample time-point. Furthermore, due to the non-supervised method of FA applied for each spectral map, factors are exclusive for each map making them independent between each time-point. For these reasons, future work will involve acquiring point spectra from multiple cells within each sample to address this variation.

Conclusion

In conclusion, confocal Raman micro-spectroscopy has proven to be a detailed, label-free, cost effective and non-destructive method of analysis to detect the uptake and fate of few-layer MoS_2 submicrometric plates inside macrophage-like cells when incubated inside a cellular micro-environment over time. The micro-environment of the MoS_2 provides information about the biochemical composition of various sub-cellular locations and indicate possible cellular processes that may be activated due to the exposure, uptake and incubation with MoS_2. This technique is transferrable for applications with different cell types and different particulate materials. A screening process for toxicology, medicine or understanding the bio-distribution and/or bio-degradation of particulate materials in-vitro could also be applied using the same method. Furthermore, Raman maps can be used to examine the cellular compartments as a function of time along with the advantage to simultaneously detect the fate of the plates once inside the cell due to no overlap with MoS_2 first order Raman bands (380 and 407 cm^{-1}) and the cellular Raman bands. It has been shown that the MoS_2 material is internalised by macrophage-like cells following a 4 h exposure and MoS_2 is still detected internally following a prolonged incubation up to 72 h. An interaction of MoS_2 with proteins could be detected in both 4 and 72 incubation time-points and are suspected of being internalised within non-lysosomal vesicles. Degradation of MoS_2 in-vitro following a 24 h incubation was recorded and vesicles are suspected of binding with lysosomes to alter the pH and cause plate dissolution. The biochemical composition of various cellular compartments was profiled illustrating both the presence of proteinaceous and lipid micro-environments. With the use of in-house datasets, it was also confirmed that vesicles present within the "perinuclear cloud" are from the phosphatidyl family of membrane lipids while Factors 1 and 4 contain the digestive enzyme lysozyme. An increase in internal lipid content as a result of MoS_2 exposure was detected using Oil Red O staining showing a saturation following a 24 h incubation with an evident decrease in lipid content following a prolonged 72 h incubation. Due to the production style of these industrial grade materials, LPS contaminants on the surface of MoS_2 plates may aid in a heightened macrophage response and contribute to the lipid production as a defense mechanism against a foreign threat.

References

1. Novoselov KS, Geim AK, Morozov S V, Jiang D, Zhang Y, Dubonos S V, et al. Electric field effect in atomically thin carbon films. Science [Internet]. 2004 Oct 22 [cited 2016 Jul 21];306(5696):666–9. Available from: http://www.ncbi.nlm.nih.gov/pubmed/15499015

2. Li X, Zhu H. Two-dimensional MoS2: Properties, preparation, and applications. J Mater. 2015;1(1):33–44.

3. Kou Z, Wang X, Yuan R, Chen H, Zhi Q, Gao L, et al. A promising gene delivery system developed from PEGylated MoS2 nanosheets for gene therapy. Nanoscale Res Lett [Internet]. 2014 [cited 2016 Jul 25];9(1):587. Available from: http://www.ncbi.nlm.nih.gov/pubmed/25386104

4. Kuhlbusch TA, Asbach C, Fissan H, Göhler D, Stintz M. Nanoparticle exposure at nanotechnology workplaces: a review. Part Fibre Toxicol [Internet]. 2011 [cited 2016 Jul 22];8:22. Available from: http://www.ncbi.nlm.nih.gov/pubmed/21794132

5. Ganatra R, Zhang Q. Few-layer MoS2: a promising layered semiconductor. ACS Nano [Internet]. 2014 May 27 [cited 2016 Sep 6];8(5):4074–99. Available from: http://www.ncbi.nlm.nih.gov/pubmed/24660756

6. Hernandez Y, Nicolosi V, Lotya M, Blighe FM, Sun Z, De S, et al. High-yield production of graphene by liquid-phase exfoliation of graphite. Nat Nanotechnol [Internet]. 2008 Sep 10 [cited 2016 Sep 12];3(9):563–8. Available from: http://www.nature.com/doifinder/10.1038/nnano.2008.215

7. Smith RJ, King PJ, Lotya M, Wirtz C, Khan U, De S, et al. Large-scale exfoliation of inorganic layered compounds in aqueous surfactant solutions. Adv Mater [Internet]. 2011;23:3944-+. Available from: http://dx.doi.org/10.1002/adma.201102584

8. Gordon S. The macrophage: Past, present and future. Eur J Immunol [Internet]. 2007 Nov [cited 2016 Aug 8];37(S1):S9–17. Available from: http://doi.wiley.com/10.1002/eji.200737638

9. Arango Duque G, Descoteaux A. Macrophage cytokines: involvement in immunity and infectious diseases. Front Immunol [Internet]. 2014 [cited 2019 Apr 8];5:491.

Available from: http://www.ncbi.nlm.nih.gov/pubmed/25339958

10. Kaufmann SHE, Dorhoi A. Molecular Determinants in Phagocyte-Bacteria Interactions. Immunity [Internet]. 2016 Mar 15 [cited 2019 Mar 12];44(3):476–91. Available from: https://www.sciencedirect.com/science/article/pii/S1074761316300528

11. Russell DG, VanderVen B, Glennie S, Mwandumba H, Heyderman R. The macrophage marches on its phagosome: dynamic assays of phagosome function. Nat Rev Immunol [Internet]. 2009 [cited 2019 Mar 11];9(8):594. Available from: https://www.ncbi.nlm.nih.gov/pmc/articles/PMC2776640/

12. Zhu X, Ji X, Kong N, Chen Y, Mahmoudi M, Xu X, et al. Intracellular Mechanistic Understanding of 2D MoS$_2$ Nanosheets for Anti-Exocytosis-Enhanced Synergistic Cancer Therapy. ACS Nano [Internet]. 2018 Mar 27 [cited 2019 Jul 31];12(3):2922–38. Available from: http://pubs.acs.org/doi/10.1021/acsnano.8b00516

13. Remmerie A, Scott CL. Macrophages and lipid metabolism. Cell Immunol [Internet]. 2018 Aug 1 [cited 2019 Mar 12];330:27–42. Available from: https://www.sciencedirect.com/science/article/pii/S0008874918300327

14. McIntyre J, Verma NK, Smith RJ, Moore C, Nerl H, McEvoy N, et al. A comparison of catabolic pathways induced in primary macrophages by pristine single walled carbon nanotubes and pristine graphene. RSC Adv [Internet]. 2016 [cited 2016 Aug 3];6(70):65299–310. Available from: http://xlink.rsc.org/?DOI=C6RA02476A

15. Chen M, Zeng G, Xu P, Lai C, Tang L. How Do Enzymes "Meet" Nanoparticles and Nanomaterials? Trends Biochem Sci [Internet]. 2017 [cited 2019 Mar 12];42(11):914–30. Available from: http://dx.doi.org/10.1016/j.tibs.2017.08.008

16. Shvedova AA, Kapralov AA, Feng WH, Kisin ER, Murray AR, Mercer RR, et al. Impaired Clearance and Enhanced Pulmonary Inflammatory/Fibrotic Response to Carbon Nanotubes in Myeloperoxidase-Deficient Mice. Mukhopadhyay P, editor. PLoS One [Internet]. 2012 Mar 30 [cited 2019 May 13];7(3):e30923. Available from: https://dx.plos.org/10.1371/journal.pone.0030923

17. Kagan VE, Konduru N V., Feng W, Allen BL, Conroy J, Volkov Y, et al. Carbon nanotubes degraded by neutrophil myeloperoxidase induce less pulmonary

inflammation. Nat Nanotechnol [Internet]. 2010 May 4 [cited 2019 May 13];5(5):354–9. Available from: http://www.nature.com/articles/nnano.2010.44

18.   Kurapati R, Mukherjee SP, Martín C, Bepete G, Vázquez E, Pénicaud A, et al. Degradation of Single-Layer and Few-Layer Graphene by Neutrophil Myeloperoxidase. Angew Chemie Int Ed [Internet]. 2018 Sep 3 [cited 2019 May 30];57(36):11722–7. Available from: http://doi.wiley.com/10.1002/anie.201806906

19.   Kurapati R, Muzi L, de Garibay APR, Russier J, Voiry D, Vacchi IA, et al. Enzymatic Biodegradability of Pristine and Functionalized Transition Metal Dichalcogenide MoS$_2$ Nanosheets. Adv Funct Mater [Internet]. 2017 Feb 1 [cited 2019 Jan 24];27(7):1605176. Available from: http://doi.wiley.com/10.1002/adfm.201605176

20.   Bhattacharya K, Mukherjee SP, Gallud A, Burkert SC, Bistarelli S, Bellucci S, et al. Biological interactions of carbon-based nanomaterials: From coronation to degradation. Nanomedicine [Internet]. 2016 Feb [cited 2019 Mar 12];12(2):333–51. Available from: http://www.ncbi.nlm.nih.gov/pubmed/26707820

21.   Suk JS, Xu Q, Kim N, Hanes J, Ensign LM. PEGylation as a strategy for improving nanoparticle-based drug and gene delivery. Adv Drug Deliv Rev [Internet]. 2016 [cited 2019 May 21];99(Pt A):28. Available from: https://www.ncbi.nlm.nih.gov/pmc/articles/PMC4798869/

22.   RAMAN C V., KRISHNAN KS. A New Type of Secondary Radiation. Nature [Internet]. 1928 Mar [cited 2019 Mar 29];121(3048):501–2. Available from: http://www.nature.com/articles/121501c0

23.   Dorney J, Bonnier F, Garcia A, Casey A, Chambers G, Byrne HJ. Identifying and localizing intracellular nanoparticles using Raman spectroscopy. Analyst [Internet]. 2012 Mar 7 [cited 2017 Oct 10];137(5):1111. Available from: http://www.ncbi.nlm.nih.gov/pubmed/22273712

24.   Byrne HJ, Bonnier F, Casey A, Maher M, McIntyre J, Efeoglu E, et al. Advancing Raman microspectroscopy for cellular and subcellular analysis: towards in vitro high-content spectralomic analysis. Appl Opt [Internet]. 2018 Aug 1 [cited 2019 Mar 13];57(22):E11. Available from: https://www.osapublishing.org/abstract.cfm?URI=ao-57-22-E11

25.   Ye M, Winslow D, Zhang D, Pandey R, Yap Y, Ye M, et al. Recent Advancement on the Optical Properties of Two-Dimensional Molybdenum Disulfide (MoS2) Thin Films. Photonics [Internet]. 2015 Mar 16 [cited 2019 Jan 24];2(1):288–307. Available from: http://www.mdpi.com/2304-6732/2/1/288

26.   Farhane Z, Bonnier F, Casey A, Maguire A, O'Neill L, Byrne HJ. Cellular discrimination using in vitro Raman micro spectroscopy: the role of the nucleolus. Analyst [Internet]. 2015 Aug 10 [cited 2019 Mar 12];140(17):5908–19. Available from: http://xlink.rsc.org/?DOI=C5AN01157D

27.   Efeoglu E, Keating M, McIntyre J, Casey A, Byrne HJ. Determination of nanoparticle localisation within subcellular organelles in vitro using Raman spectroscopy. Anal Methods [Internet]. 2015 Nov 19 [cited 2017 Oct 10];7(23):10000–17. Available from: http://xlink.rsc.org/?DOI=C5AY02661J

28.   Blanco É, Afanasiev P, Berhault G, Uzio D, Loridant S. Resonance Raman spectroscopy as a probe of the crystallite size of MoS2 nanoparticles. Comptes Rendus Chim [Internet]. 2016 Oct 1 [cited 2019 Jan 24];19(10):1310–4. Available from: https://www.sciencedirect.com/science/article/pii/S1631074816000254

29.   Mercado E, Goodyear A, Moffat J, Cooke M, Sundaram RS. A Raman metrology approach to quality control of 2D MoS $_2$ film fabrication. J Phys D Appl Phys [Internet]. 2017 May 10 [cited 2017 Aug 30];50(18):184005. Available from: http://stacks.iop.org/0022-3727/50/i=18/a=184005?key=crossref.d57ce00e9e67dafd9f8f1f5e1473f5f8

30.   Lee C, Yan H, Brus LE, Heinz TF, Hone J, Ryu S. Anomalous Lattice Vibrations of Single and Few-Layer MoS 2. [cited 2017 Sep 11]; Available from: https://arxiv.org/ftp/arxiv/papers/1005/1005.2509.pdf

31.   Placidi M, Dimitrievska M, Izquierdo-Roca V, Fontané X, Castellanos-Gomez A, Pérez-Tomás A, et al. Multiwavelength excitation Raman scattering analysis of bulk and two-dimensional MoS $_2$: vibrational properties of atomically thin MoS $_2$ layers. 2D Mater [Internet]. 2015 Jul 7 [cited 2019 Feb 19];2(3):035006. Available from: http://stacks.iop.org/2053-1583/2/i=3/a=035006?key=crossref.8b0293927d7a8008e269ac49ec8843db

32. Backes C, Szydłowska BM, Harvey A, Yuan S, Vega-Mayoral V, Davies BR, et al. Production of highly monolayer enriched dispersions of liquid-exfoliated nanosheets by liquid cascade centrifugation. ACS Nano. 2016 Jan 26;10(1):1589–601.

33. Backes C, Smith RJ, McEvoy N, Berner NC, McCloskey D, Nerl HC, et al. Edge and confinement effects allow in situ measurement of size and thickness of liquid-exfoliated nanosheets. Nat Commun. 2014 Aug 7;5.

34. Moore C, Movia D, Smith RJ, Hanlon D, Lebre F, Lavelle EC, et al. Industrial grade 2D molybdenum disulphide (MoS $_2$): an *in vitro* exploration of the impact on cellular uptake, cytotoxicity, and inflammation. 2D Mater [Internet]. 2017 Apr 3 [cited 2017 Jun 14];4(2):025065. Available from: http://stacks.iop.org/2053-1583/4/i=2/a=025065?key=crossref.f9ed1e670cfd666e614042f5b079ad20

35. Wick P, Louw-Gaume AE, Kucki M, Krug HF, Kostarelos K, Fadeel B, et al. Classification Framework for Graphene-Based Materials. Angew Chemie Int Ed [Internet]. 2014 Jul 21 [cited 2019 Nov 13];53(30):7714–8. Available from: http://doi.wiley.com/10.1002/anie.201403335

36. Bianco A, Cheng HM, Enoki T, Gogotsi Y, Hurt RH, Koratkar N, et al. All in the graphene family - A recommended nomenclature for two-dimensional carbon materials. Vol. 65, Carbon. Elsevier Ltd; 2013. p. 1–6.

37. Gautier A, Juillerat A, Heinis C, Corrêa IR, Kindermann M, Beaufils F, et al. An engineered protein tag for multiprotein labeling in living cells. Chem Biol [Internet]. 2008 Feb [cited 2019 Apr 10];15(2):128–36. Available from: http://www.ncbi.nlm.nih.gov/pubmed/18291317

38. Coleman JN, Lotya M, O'Neill A, Bergin SD, King PJ, Khan U, et al. Two-dimensional nanosheets produced by liquid exfoliation of layered materials. Science. 2011;331(6017):568–71.

39. Khan U, Porwal H, Óneill A, Nawaz K, May P, Coleman JN. Solvent-exfoliated graphene at extremely high concentration. Langmuir. 2011;27(15):9077–82.

40. Varrla E, Backes C, Paton KR, Harvey A, Gholamvand Z, McCauley J, et al. Large-Scale Production of Size-Controlled MoS $_2$ Nanosheets by Shear Exfoliation. Chem Mater [Internet]. 2015 Feb 10 [cited 2016 Sep 12];27(3):1129–39. Available from:

http://pubs.acs.org/doi/abs/10.1021/cm5044864

41. Kerr LT, Byrne HJ, Hennelly BM. Optimal choice of sample substrate and laser wavelength for Raman spectroscopic analysis of biological specimen. Anal Methods [Internet]. 2015 Jun 11 [cited 2019 Jan 28];7(12):5041–52. Available from: http://xlink.rsc.org/?DOI=C5AY00327J

42. Keating ME, Bonnier F, Byrne HJ. Spectral cross-correlation as a supervised approach for the analysis of complex Raman datasets: the case of nanoparticles in biological cells. Analyst [Internet]. 2012 Nov 12 [cited 2019 Jan 28];137(24):5792. Available from: http://xlink.rsc.org/?DOI=c2an36169h

43. Movasaghi Z, Rehman S, Rehman IU. Raman Spectroscopy of Biological Tissues. Appl Spectrosc Rev [Internet]. 2007 Sep [cited 2019 Jan 28];42(5):493–541. Available from: http://www.tandfonline.com/doi/abs/10.1080/05704920701551530

44. ACS Material. Bio MoS2 - Graphene-like Materials - Materials [Internet]. [cited 2019 Jan 24]. Available from: https://www.acsmaterial.com/bio-mos2.html

45. Vlasova II, Kapralov AA, Michael ZP, Burkert SC, Shurin MR, Star A, et al. Enzymatic oxidative biodegradation of nanoparticles: Mechanisms, significance and applications. Toxicol Appl Pharmacol [Internet]. 2016 May 15 [cited 2019 May 21];299:58–69. Available from: http://www.ncbi.nlm.nih.gov/pubmed/26768553

46. Dellibovi-Ragheb T, Altan-Bonnet N. Cloud storage for endosomes. EMBO J [Internet]. 2016 Aug 15 [cited 2019 May 17];35(16):1724–5. Available from: http://www.ncbi.nlm.nih.gov/pubmed/27378788

47. Malini R, Venkatakrishna K, Kurien J, M. Pai K, Rao L, Kartha VB, et al. Discrimination of normal, inflammatory, premalignant, and malignant oral tissue: A Raman spectroscopy study. Biopolymers [Internet]. 2006 Feb 15 [cited 2019 Mar 13];81(3):179–93. Available from: http://doi.wiley.com/10.1002/bip.20398

48. Berg JM, Tymoczko JL, Stryer L. Lipids and Cell Membranes. In: Biochemistry [Internet]. 5th ed. W H Freeman; 2002 [cited 2019 May 30]. Available from: https://www.ncbi.nlm.nih.gov/books/NBK22361/

49. Zhang C, Wang Y, Wang F, Wang Z, Lu Y, Xu Y, et al. Quantitative profiling of

glycerophospholipids during mouse and human macrophage differentiation using targeted mass spectrometry. Sci Rep [Internet]. 2017 Dec 24 [cited 2019 May 30];7(1):412. Available from: http://www.nature.com/articles/s41598-017-00341-2

50.   Cheng M, Pan H, Dai Y, Zhang J, Tong Y, Huang Y, et al. Phosphatidylcholine regulates NF-κB activation in attenuation of LPS-induced inflammation: evidence from in vitro study. Animal Cells Syst (Seoul) [Internet]. 2018 Jan 2 [cited 2019 May 31];22(1):7–14. Available from: https://www.tandfonline.com/doi/full/10.1080/19768354.2017.1405072

51.   Keshav S, Chung P, Milon G, Gordon S. Lysozyme is an inducible marker of macrophage activation in murine tissues as demonstrated by in situ hybridization. J Exp Med [Internet]. 1991 Nov 1 [cited 2019 May 21];174(5):1049–58. Available from: http://www.ncbi.nlm.nih.gov/pubmed/1940787

52.   Davis KM, Weiser JN. Modifications to the peptidoglycan backbone help bacteria to establish infection. Infect Immun [Internet]. 2011 Feb 1 [cited 2019 May 30];79(2):562–70. Available from: http://www.ncbi.nlm.nih.gov/pubmed/21041496

53.   Walther TC, Farese R V, Jr. The life of lipid droplets. Biochim Biophys Acta [Internet]. 2009 Jun [cited 2019 May 22];1791(6):459–66. Available from: http://www.ncbi.nlm.nih.gov/pubmed/19041421

54.   Hayman YA, Sadofsky LR, Williamson JD, Hart SP, Morice AH. The effects of exogenous lipid on THP-1 cells: an in vitro model of airway aspiration? ERJ open Res [Internet]. 2017 Jan [cited 2019 Mar 13];3(1). Available from: http://www.ncbi.nlm.nih.gov/pubmed/28344981

55.   Teng O, Ang CKE, Guan XL. Macrophage–Bacteria Interactions—A Lipid-Centric Relationship. Front Immunol [Internet]. 2017 Dec 20 [cited 2019 May 21];8:1836. Available from: http://journal.frontiersin.org/article/10.3389/fimmu.2017.01836/full

56.   White JR, Chait A, Klebanoff SJ, Deeb S, Brunzell JD. Bacterial lipopolysaccharide reduces macrophage lipoprotein lipase levels: an effect that is independent of tumor necrosis factor [Internet]. [cited 2019 Jan 24]. Available from: www.jlr.org

57.   Melo RCN, Dvorak AM. Lipid body-phagosome interaction in macrophages during infectious diseases: host defense or pathogen survival strategy? PLoS Pathog

[Internet]. 2012 [cited 2019 May 31];8(7):e1002729. Available from: http://www.ncbi.nlm.nih.gov/pubmed/22792061

58.   Tang ACL, Hwang G-L, Tsai S-J, Chang M-Y, Tang ZCW, Tsai M-D, et al. Biosafety of Non-Surface Modified Carbon Nanocapsules as a Potential Alternative to Carbon Nanotubes for Drug Delivery Purposes. Chin W-C, editor. PLoS One [Internet]. 2012 Mar 22 [cited 2019 Sep 3];7(3):e32893. Available from: http://www.ncbi.nlm.nih.gov/pubmed/22457723

59.   Lux C de G, Joshi-Barr S, Nguyen T, Mahmoud E, Schopf E, Fomina N, et al. Biocompatible polymeric nanoparticles degrade and release cargo in response to biologically relevant levels of hydrogen peroxide. J Am Chem Soc [Internet]. 2012 Sep 26 [cited 2019 Jul 31];134(38):15758. Available from: http://www.ncbi.nlm.nih.gov/pubmed/22946840

60.   Wang Z, von dem Bussche A, Qiu Y, Valentin TM, Gion K, Kane AB, et al. Chemical Dissolution Pathways of MoS_2 Nanosheets in Biological and Environmental Media. Environ Sci Technol [Internet]. 2016 Jul 5 [cited 2019 Jul 31];50(13):7208–17. Available from: http://pubs.acs.org/doi/10.1021/acs.est.6b01881

61.   Lukasiewicz J, Lugowski C. Editorial: O-specific polysaccharide confers lysozyme resistance to extraintestinal pathogenic Escherichia coli. Virulence [Internet]. 2018 [cited 2019 May 21];9(1):919–22. Available from: http://www.ncbi.nlm.nih.gov/pubmed/29638195

62.   Behzadi S, Serpooshan V, Tao W, Hamaly MA, Alkawareek MY, Dreaden EC, et al. Cellular uptake of nanoparticles: journey inside the cell. Chem Soc Rev [Internet]. 2017 Jul 17 [cited 2019 Jul 31];46(14):4218–44. Available from: http://www.ncbi.nlm.nih.gov/pubmed/28585944

63.   von Moos N, Bowen P, Slaveykova VI. Bioavailability of inorganic nanoparticles to planktonic bacteria and aquatic microalgae in freshwater. Environ Sci Nano [Internet]. 2014 May 19 [cited 2019 Jul 31];1(3):214. Available from: http://xlink.rsc.org/?DOI=c3en00054k

64.   Voeltz GK, Rolls MM, Rapoport TA. Structural organization of the endoplasmic reticulum. EMBO Rep [Internet]. 2002 Oct [cited 2019 May 3];3(10):944–50.

Available from: http://www.ncbi.nlm.nih.gov/pubmed/12370207

65.   Murphy DJ. The biogenesis and functions of lipid bodies in animals, plants and microorganisms. Prog Lipid Res [Internet]. 2001 Sep 1 [cited 2019 May 3];40(5):325–438. Available from: https://www.sciencedirect.com/science/article/pii/S0163782701000133?via%3Dihub

66.   Melo RCN, D'Avila H, Wan H-C, Bozza PT, Dvorak AM, Weller PF. Lipid bodies in inflammatory cells: structure, function, and current imaging techniques. J Histochem Cytochem [Internet]. 2011 May [cited 2019 May 3];59(5):540–56. Available from: http://www.ncbi.nlm.nih.gov/pubmed/21430261

67.   Pacheco P, Vieira-de-Abreu A, Gomes RN, Barbosa-Lima G, Wermelinger LB, Maya-Monteiro CM, et al. Monocyte Chemoattractant Protein-1/CC Chemokine Ligand 2 Controls Microtubule-Driven Biogenesis and Leukotriene B4-Synthesizing Function of Macrophage Lipid Bodies Elicited by Innate Immune Response. J Immunol [Internet]. 2007 Dec 15 [cited 2019 May 22];179(12):8500–8. Available from: http://www.ncbi.nlm.nih.gov/pubmed/18056397

68.   Slocum C, Coats SR, Hua N, Kramer C, Papadopoulos G, Weinberg EO, et al. Distinct Lipid A Moieties Contribute to Pathogen-Induced Site-Specific Vascular Inflammation. Gunn JS, editor. PLoS Pathog [Internet]. 2014 Jul 10 [cited 2016 Aug 4];10(7):e1004215. Available from: http://dx.plos.org/10.1371/journal.ppat.1004215

69.   Martinez FO, Gordon S. The M1 and M2 paradigm of macrophage activation: time for reassessment. F1000Prime Rep [Internet]. 2014 [cited 2019 Mar 11];6:13. Available from: http://www.ncbi.nlm.nih.gov/pubmed/24669294

70.   Genin M, Clement F, Fattaccioli A, Raes M, Michiels C. M1 and M2 macrophages derived from THP-1 cells differentially modulate the response of cancer cells to etoposide. BMC Cancer [Internet]. 2015 Aug 8 [cited 2019 Mar 11];15:577. Available from: http://www.ncbi.nlm.nih.gov/pubmed/26253167

71.   Fujihara M, Muroi M, Tanamoto K, Suzuki T, Azuma H, Ikeda H. Molecular mechanisms of macrophage activation and deactivation by lipopolysaccharide: roles of the receptor complex. Pharmacol Ther [Internet]. 2003 Nov 1 [cited 2019 Feb 22];100(2):171–94. Available from:

https://www.sciencedirect.com/science/article/pii/S0163725803001220

72. Stiebing C, Schmölz L, Wallert M, Matthäus C, Lorkowski S, Popp J. Raman imaging of macrophages incubated with triglyceride-enriched oxLDL visualizes translocation of lipids between endocytic vesicles and lipid droplets. J Lipid Res [Internet]. 2017 [cited 2019 Jan 30];58(5):876–83. Available from: http://www.ncbi.nlm.nih.gov/pubmed/28143895

73. Feingold KR, Shigenaga JK, Kazemi MR, McDonald CM, Patzek SM, Cross AS, et al. Mechanisms of triglyceride accumulation in activated macrophages. J Leukoc Biol [Internet]. 2012 Oct 1 [cited 2019 Mar 12];92(4):829–39. Available from: http://doi.wiley.com/10.1189/jlb.1111537

74. Meng F, Lowell CA. Lipopolysaccharide (LPS)-induced macrophage activation and signal transduction in the absence of Src-family kinases Hck, Fgr, and Lyn. J Exp Med [Internet]. 1997 May 5 [cited 2019 Mar 12];185(9):1661–70. Available from: http://www.ncbi.nlm.nih.gov/pubmed/9151903

75. Al-Shabany AJ, Moody AJ, Foey AD, Billington RA. Intracellular NAD+ levels are associated with LPS-induced TNF-α release in pro-inflammatory macrophages. Biosci Rep [Internet]. 2016 Jan 13 [cited 2019 Jan 24];36(1):e00301. Available from: http://www.ncbi.nlm.nih.gov/pubmed/26764408

76. Santucci P, Bouzid F, Smichi N, Poncin I, Kremer L, De Chastellier C, et al. Experimental models of foamy macrophages and approaches for dissecting the mechanisms of lipid accumulation and consumption during dormancy and reactivation of tuberculosis. Vol. 6, Frontiers in Cellular and Infection Microbiology. Frontiers Media S.A.; 2016.